Universidad de La Laguna

Facultad de Ciencias

Departamento de Astrofísica

THE CONNECTION BETWEEN THE OVERALL STRUCTURE OF DISC GALAXIES AND NUCLEAR RINGS AND SPIRALS

MASTER'S DEGREE IN ASTROPHYSICS

Master's thesis by

Pablo Jiménez Sánchez

Supervised by

Sébastien Comerón Limbourg

Almudena Prieto Escudero

July 2024

Contents

Resumen

Los anillos nucleares o circumnucleares son estructuras cerradas o casi cerradas, circulares o cuasi-circulares hechas de material gaseoso o estrellas que pueden aparecer en las regiones más centrales de algunas galaxias y a menudo presentan una elevada tasa de formación estelar. Esto los convierte en trazadores de poblaciones estelares jóvenes y de recientes afluencias de gas a la zona central de la galaxia. Su estudio es clave a la hora de revelar los procesos que influencian la evolución de las regiones centrales de galaxias y pueden contiener pistas importantes sobre la evolución y la dinámica de las mismas.

En este trabajo presentamos el análisis de los anillos nucleares presentes en una selección de 52 anillos nucleares presentes en AINUR (Atlas of Images of NUclear Rings). El objetivo de AINUR era recoger y caracterizar todos aquellos anillos nucleares presentes en la muestra de Ho et al. (1995) que hubieran sido observados por el *Telescopio Espacial Hubble*. El catálogo de AINUR fue extendido con anillos encontrados en la literatura. Nosotros hemos escogido únicamente aquellos anillos observados en el óptico por los instrumentos de alta resolución y gran amplitud de campo disponibles en el *Telescopio Espacial Hubble*, en concreto y, por orden de mayor a menor resolución angular, ACS/WFC (Advance Camera for Surveys/ Wide Field Camera), WFC3/UVIS (Wide Field Camera 3, canal óptico y ultravioleta) y WFPC2 (Wide Field Planetary Camera 2). Hemos escogido como ventana espectral de trabajo el rango de radiación visible, ya que nos permite observar las estrellas, la absorción del polvo y las zonas de formación estelar.

Para estudiar la estructura interior de las galaxias de la muestra hemos recurrido a la técnica conocida como unsharp-masking. Este método consiste en la creación de imágenes que muestran con un alto constrante información sobre estructuras subyacentes en la galaxia -regiones de formación estelar, brazos espirales, filamentos de polvo, etc.- que normalmente quedan ocultos por la luz de las poblaciones estelares más brillantes de la galaxia. El proceso de creación de esta imagen consiste en la división de la imagen original por el resultado de la convolución entre dicha imagen y un kernel gaussiano. Para las imágenes de nuestra muestra, hemos comprobado que un kernel gaussiano con una sigma de 15 a 30 píxeles produce los mejores resultados, siendo 20 píxeles el valor utilizado para la mayoría de la muestra, lo que representa entre 1 y 2 segundos de arco según el instrumento. La combinación de la técnica de unsharp-masking con imágenes de alta resolución espacial procedentes del archivo del *Telescopio Espacial Hubble* nos permite realizar un análisis de la región nuclear de las galaxias en nuestra muestra.

Nuestro objetivo es buscar correlaciones entre la estructura de la galaxia a gran escala y el anillo nuclear que hospedan, con el fin de desvelar cuestiones acerca del origen y el rol de los anillos nucleares en la evolución galáctica.

Hemos dividido los anillos nucleares presentes en nuestra muestra en 3 clases, en función de la apariencia de la estructura subyacente: anillos two-armed, anillos 2 arms+ y anillos many-armed. La primera clase contiene anillos nucleares que presentan dos canales o filamentos de polvo simétricas que llegan hasta el anillo. La segunda clase es similar a la anterior, añadiendo a los dos caminos principales de polvo, otras líneas más pequeñas y delgadas que se acercan al anillo. La última clase contiene aquellos anillos con muchos brazos de polvo acercándose a él en los que no se observa la prevalencia de ninguno de ellos ni una simetría clara en su estructura.

Las galaxias han sido clasificadas según su morfología aparente en dos clasificaciones distin-

tas. Una de ellas está basada en trabajos anteriores de la literatura, dividiendo las galaxias en Grand Design, Multiarmed y Flocculent. Las galaxias Grand Design tienen una estructura muy definida, con dos brazos espirales claramente delineados que rodean un núcleo bien determinado, las galaxias Multiarmed contienen varios brazos espirales prevalentes largos y continuos y las galaxias Flocculent se caracterizan por su estructura de polvo y otro material caótica y fragmentada con brazos cortos. La segunda clasificación es una división original de nuestro trabajo, sitúa las galaxias en tres grupos basado en lo compacto de la estructura espiral de los brazos alrededor del anillo nuclear, un grupo para aquellas con la estructura más compacta, otro para aquellas con la estructura menos densa y un último grupo para las galaxias que se sitúan en un caso intermedio a los anteriores.

Por medio de estas clasificaciones hemos encontrado que los anillos two-armed son más comúnes en galaxias de un tipo más tardío, con barras fuertes y clasificadas como Grand Design; mientras que los anillos many-armed son más frecuentes en galaxias de tipo más tardío no barradas clasificadas como Flocculent o Multiarm. Los anillos 2 arms+ representan un caso intermedio entre los otros dos, son más comunes en galaxias Multiarm de tipo más tardío con barras débiles. Hemos concluido que la intensidad de la barra y su impacto en la simetría de 180^{o} que presenta el potencial gravitatorio resultante determina la morfología del anillo nuclear que se forma en el centro.

La técnica de unsharp-masking nos permite seguir los canales de polvo que transportan material desde las zonas más externas de la galaxia hasta aquellas más internas, donde hemos encontrado que 28 de las galaxias presentes en nuestra muestra presentan una estructura espiral en el interior del anillo nuclear. Este tipo de estructura se asocia con flujos de gas frío que alimentan el agujero negro central. La aparición de estas estructuras no parece verse favorecida por ningún rango de masa estelar o tipo morfológico de Hubble de la galaxia anfitrión, aunque son más comunes en galaxias barradas. Las espirales nucleares se pueden encontrar en el interior de cualquier tipo de anillo y muestran una preferencia hacia galaxias Grand Design y aquellas con la estructura central de brazos espirales menos compacta. Hemos encontrado estas formaciones en la inmensa mayoría de las galaxias de nuestra muestra para las cuales disponíamos de una imagen del *Telescopio Espacial Hubble* que mostrara el interior del anillo nuclear con la suficiente resolución angular, lo que sugiere que se trata de un fenómeno frecuente en galaxias con anillos nucleares de formación estelar.

Abstract

Nuclear or circumnuclear rings are closed or nearly closed, circular or almost circular structures made of gaseous material or stars that can appear in the central regions of some galaxies and often showcase enhanced star formation. They are tracers of young circumnuclear populations and recent gas inflows, and they play an important role in the evolution of barred galaxies. their study is then key in unveiling the processes that take part in their formation and in the evolution of the central part of galaxies and may hold important clues about the overall evolution and dynamics of galaxies.

We present a study of the nuclear rings in a selection of nuclear rings from the Atlas of Images of NUclear Rings (AINUR). In order to study the inner structure of these galaxies we have produced unsharp-masked images of their nuclear regions from *Hubble Space Telescope* archival data.

We aim to check for correlations between known galactic properties and the morphology of nuclear rings to unveil questions about the origin and role in galactic evolution.

The nuclear rings in our sample have been divided in 3 classes depending on their morphology: two-armed, 2 arms+ and many-armed rings, based on the amount a symmetry of the dust lanes that reach into the ring. We made two distinct morphology classifications for the host galaxies. We classified the overall morphology of the galaxies based on previous works from the literature that divides galaxies in Grand Design, Multiarmed and Flocculent. We also devised an original visual classification that divides galaxies in three groups based on the compactness of the arm structure that surrounds the ring.

We found that two-armed rings are more common in later type Grand Design galaxies featuring strong bars and that many-armed rings are more common in later type Flocculent and Multiarmed unbarred galaxies. 2arms+ rings represent an intermediate case between the other two classes, appearing more often in Multiarmed galaxies with weak bars. We concluded that the bar strength and its impact in the 180^{o} symmetric potential determine the morphology of the nuclear ring.

The unsharp-mask technique allows us to follow up the channels of dust carrying material from the outer sections of the galaxy to the innermost regions, where we found that 28 of the galaxies in our sample exhibit a nuclear spiral structure in the inside of the nuclear ring they host. This kind of structure is associated with cold dust inflows that feed the very low sub-Eddington regime Black Hole that usually resides in the very centre of these galaxies. The appearance of these structures does not seem to be favoured in any particular stellar mass range or Hubble stage of the host, although they more common in barred galaxies. They can be found in any kind of ring, and they do show a preference towards Grand Design galaxies and the galaxies with the least compact central arm structure. We found nuclear spirals in almost every galaxy from our sample for which we had an *HST* image displaying the interior of the nuclear ring properly resolved available, which suggests that it is a rather frequent phenomenon in galaxies featuring nuclear rings.

1 Introduction

Nuclear or circumnuclear rings are closed, or nearly closed, circular, or almost circular structures made out of gaseous material and/or stars that can appear in the central regions of some galaxies and often showcase enhanced star formation. They were first observed in the galaxy NGC 4321 by Keeler (1908) and first described in the study of NGC 3351 by Curtis (1918).

Nuclear rings are especially bright and their origin is believed to be linked to an inflow of said gaseous material towards the centre of the galaxy, this streaming motion would be caused by the loss of angular momentum (Combes & Gerin 1985). The change in momentum is caused by the presence of non-symmetric morphological features such as bars (see e.g. Shlosman et al. 1990; Athanassoula 1994; Combes 2001). Thus, a connection between nuclear rings and Inner Lindblad Resonances (ILRs) arise, after dynamical shocks carry the gas towards the centre following radial orbits, the material crosses the ILR and the trajectory begins to shift from radial to circular (Comerón et al. 2010). As proposed by Combes (1996), the location of nuclear rings corresponds to the space between the outer and the inner ILR for galaxies that feature both, and inside the single ILR when the galaxy has only one of them (see e.g. Shlosman 1999; Sheth et al. 2000), which serves as a trapping mechanism of the ring material. However, numerical results from Kim et al. (2012) suggest that a ring is formed because of the centrifugal barrier that the migrating material feels, later shrinking in size as gas with lower angular momentum is added, claiming that the location of the ring between two ILRs is a coincidence. The exact radius (relative to the ILRs) at which a nuclear ring may form is still not a closed subject (see e.g. the introduction of van de Ven & Chang 2009).

Nevertheless, the fact that rings consist of gas migrating from outer parts inward is a certainty, even if the connection with ILRs could be disputed. Therefore, nuclear rings become tracers of recent gas inflow to the circumnuclear region (Knapen et al. 1995).

Nuclear rings are very stable and long-lived structures (Knapen et al. 2006), which allows the molecular gas accumulating within to become sufficiently dense to initiate star formation. This makes them useful tracers of young circumnuclear populations, and thus a crucial element in the study of secular evolution (Comerón et al. 2008). They also play an important role in the evolution of barred galaxies, as they often act as a site of active star formation near the centres, (see Buta 1986; Garcia-Barreto et al. 1991; Barth et al. 1995; Maoz et al. 2001; Mazzuca et al. 2008).

The study of nuclear rings is crucial in unveiling the processes that take part in their formation and in the evolution of the central region of galaxies and may hold important clues about the evolution and dynamics of galaxies.

1.1 AINUR

This work was conceived as a continuation of the previous work by Comerón et al. (2010), AINUR (Atlas of Images of NUclear Rings). AINUR includes 113 rings found in 107 galaxies, and a deep study of these rings aiming to explore possible relationships between the size and morphology of the rings and various galactic parameters.

AINUR follows the path of previous Atlas, the likes of Sérsic & Pastoriza (1965), Pogge (1989), Buta & Crocker (1993), Knapen, Pérez-Ramírez, & Laine (2002) or Knapen (2005), but taking advantage of the high resolution provided by the *Hubble Space Telescope (HST)* to study the intermediate and small-sized nuclear rings. AINUR presents a pioneering work about a uniform and comprehensive study of every nuclear ring using *HST* imaging, as previous efforts had focused on either individual or small groups of rings.

The galaxy sample in AINUR is mainly based on the survey by Ho et al. (1995) aimed at 'dwarf' Seyfert nuclei in nearby galaxies in order to check for correlations between the ring properties and Active Galactic Nuclei (no correlation was found).

The initial sample was selected satisfying the following criteria:

(i) $B_{\rm T} \leq 12.5$ in the RC3;

(ii) not catalogued as edge-on in the RC3;

(iii) axial ratio $d/D > 0.35$ in the HYPERLEDA data base;

(iv) not a Milky Way satellite;

(v) imaged by *HST* with one or more of the following cameras: ACS, FOC, NICMOS, WFPC2.

The sample was then expanded with a selected group of nuclear rings from the literature.

The study conducted in AINUR concludes that star-forming nuclear rings are found in 20 ± 2 per cent of disc galaxies in the range of Hubble morphological types $-3 < T \leq 7$, implying an effective nuclear ring lifetime of $2-3$ Gyr, in broad agreement with a large range of other observational and numerical studies. Additionally, they found that the size of nuclear rings seems to be constrained by the size and ellipticity of bars, a correlation later confirmed by Erwin (2024).

They also observed that star-forming rings are predominantly found in galaxies with morphological types ranging from S0 to Sc and show no strong preference for barred host galaxies.

In this paper, we aspire to expand upon the work from AINUR by taking a closer look on star-forming nuclear rings, their differences from one another and the properties of their host galaxies that may cause these differences. To achieve this, enhanced the structure of nuclear rings through the use of the unsharp-masking technique. This allowed us to distinguish different classes of rings based on their structure, and to check for correlations with known properties of the hosts.

1.2 Galaxy morphology

The study of galaxies and their properties finds its root in the morphological classification. The progress in this field can be traced back to the work by Hubble (1926), later expanded on by de Vaucouleurs (1959) and Sandage (1961). The classical morphological classification present in this paper comes from the work by Buta et al. (2007), which is a modern revision of the classification from de Vaucouleurs.

The main interests of our work in the classical morphology studies lies on two aspects: the stage, which refers to the E-S0-S-I position along a modified Hubble sequence, and the family, referring to the presence or absence of a bar (see Buta et al. 2015).

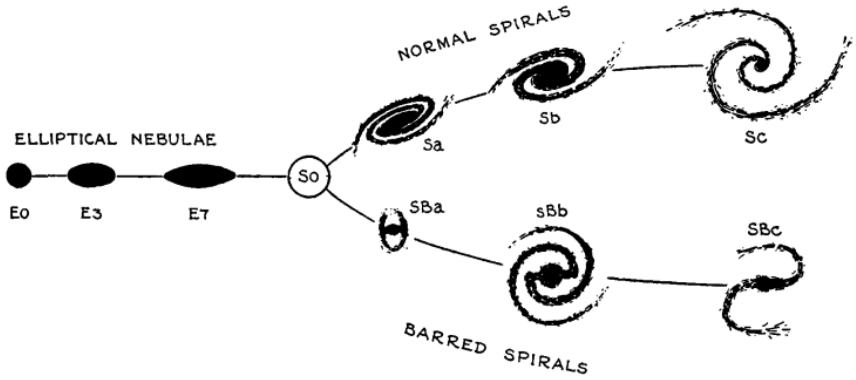

Figure 1: The Hubble sequence, as it appears in Hubble (1936).

For spiral galaxies, the Hubble stage describes the tightness of the spiral arm structure. In this work the galaxies are found in the range between S0 and Scd. The galaxies are divided in three families regarding the presence of a bar: SB for barred galaxies, SAB for weakly barred galaxies and SA for non-barred galaxies.

The connection between nuclear rings and morphological classes has been studied previously in AINUR (Comerón et al. 2010).

We aim to draw connections between the different galaxy stages and families and the different ring classes according to a nuclear ring morphological classification that we describe in Sect. 4.

1.3 Channels of material towards the centre

This work employs the unsharp-masking technique on high-angular-resolution images from the *Hubble Space Telescope* to examine the channels of dust carrying material from the outer sections of the galaxy to the central black hole.

The processes responsible for the loss of angular momentum and the subsequent fall of the

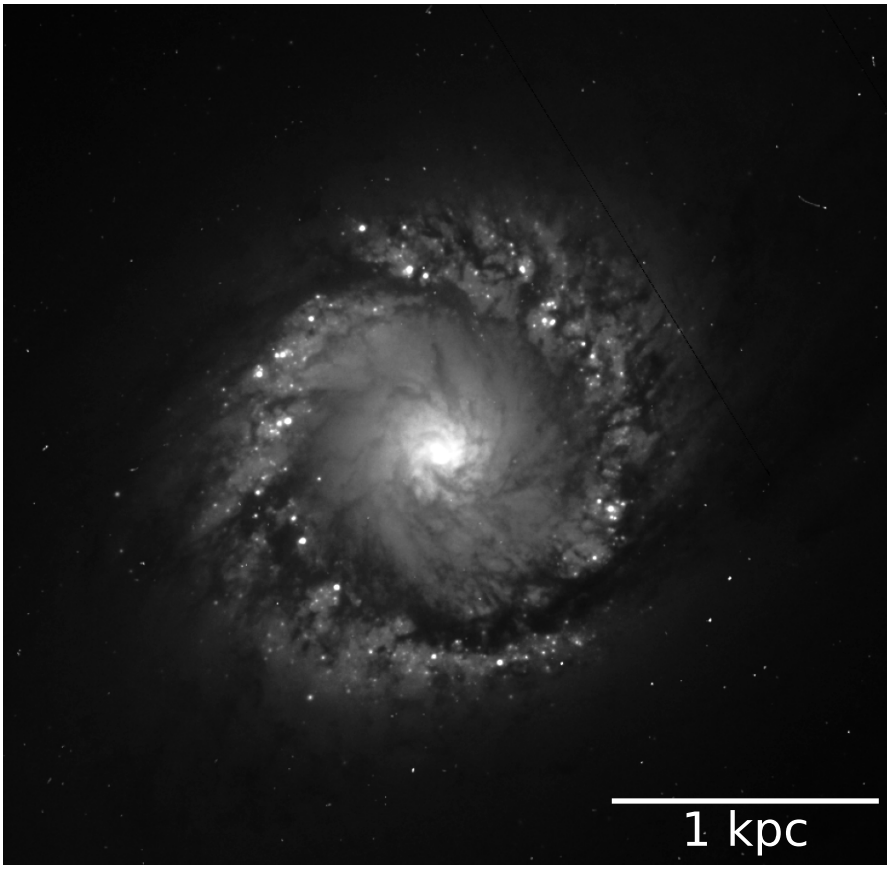

Figure 2: Nuclear ring and nuclear spiral in the centre of NGC 1097. Image taken by the ACS/WFC from the *HST* using the *F814W* filter.

material towards the centre remain a matter of controversy (see review in the introduction by Comerón et al. 2021). The mechanisms that are capable of generating torques able to cause the velocity losses include galaxy-galaxy interactions (Negroponte & White 1983) and shocks associated with bars (Athanassoula 1992) and spiral arms (Kim & Kim 2014). Within the 1 kpc radius, the process of angular momentum loss remains a mystery, and suggestions about this topic centre around the idea of bars within bars (Shlosman et al. 1989; Querejeta et al. 2016) and nuclear spirals (Kim & Elmegreen 2017).

In this work, we take a closer look at the central kiloparsec with a focus on nuclear spirals, the morphology of nuclear rings that present these structures and the galaxies that host them.

Nuclear spirals are a network of long, narrow, dust filaments that spiral inward as they get closer to the centre, they have been previously observed in multiple objects, some of them featured in this work, such as NGC 1097 (Prieto et al. 2005, 2021), NGC 6951 (Storchi-Bergmann et al. 2007, their Figure 2), ESO 428-G14 (see Figure 8 of Prieto et al. 2014; May et al. 2018), NGC 1566 (Prieto et al. 2021, their Figure 4) and M31 (Alig et al. 2023). Prieto et al. (2005) shows that

these filaments are channels for cold dust and gas to reach the centre. The spiral propagation may be caused by different dynamical conditions in the off-plane gas and the evidence suggests that it corresponds to a shock with strong shear. Alig et al. (2023) uses hydrodynamical simulations to study the innermost structure of M31, reaching the conclusion that these filaments are the main contributors to the inflow rate of the central BH (black hole) for those in the very low sub-Eddington regime, and the consequence is a low accretion mode of the BH.

Studying the innermost region of the galaxies may allow us to uncover mysteries about the transportation of gas and material towards the centre and the role of nuclear rings in this process.

2 Sample and image selection

The sample is composed of galaxies taken from AINUR (Comerón et al. 2010), the complete original sample features 107 galaxies that exhibit nuclear rings. From that work, we have chosen those galaxies that show star-forming nuclear rings and have been properly observed by the *Hubble Space Telescope* so that the follow-through structure analysis could be performed. The restriction of our work to *HST* images is a result of our desire to study the inner structure of these objects with high angular resolution. The dimensions of nuclear rings are usually within the range of hundreds of parsecs, in consequence, the pursue of this task demands the use of images that reach an angular resolution corresponding to tens of parsecs, only available for space telescopes and telescopes with adaptive optics.

After removing those galaxies with dust rings, and those for which there is no *HST* image in the optical range that shows the nuclear area or that have not been pictured by the *HST* altogether, the final sample is composed of 52 galaxies.

During the sample selection process we looked for the image with the largest field of view available for each object. This makes the ACS/WFC (Advance Camera for Surveys/ Wide Field Camera) the highest prioritised instrument available, with a field of view of $202'' \times 202''$ and a pixel scale of $0''.05$ per pixel; followed by the WFC3/UVIS (Wide Field Camera 3, UV and optical channel), one of the latest installed instruments , that can cover $160'' \times 160''$, $0''.04$ per pixel; and at last, although heavily featured due to its extended use, is WFPC2 (Wide Field Planetary Camera 2), that uses a mosaic of 3 CCDs with a coverage of $80'' \times 80''$, $0''.0996$ per pixel and a fourth smaller CCD with a coverage of $36'' \times 36''$, $0''.0455$ per pixel.

We have chosen optical radiation for our work since it allows to observe stars, dust and star formation. Most of the selected images were taken using the *F814W* filter, a wide range filter centered in 814 nm and the rest were taken using *F606W*, centered in 606 nm and *F706W*, centered in 706 nm.

2.1 Incompleteness and bias

The most limiting source of incompleteness of our sample is inherited from the challenges and limitations of the original sample from AINUR, such as the unavailability of high quality imaging for a large number of known nuclear ring hosts. The original work suffers from an obvious bias towards nearby galaxies on account of their visibility and our resolving power; which makes the observation of small nuclear rings is impossible for distant galaxies.

The main root of disparity between the size of our final sample and that of AINUR comes from our complete dedication to *HST* images. AINUR aimed at including all known nuclear rings, even those only observed by ground-based telescopes, while we have discarded nuclear rings that would otherwise have been fit for our analysis have been rejected due to their absence in the *HST*

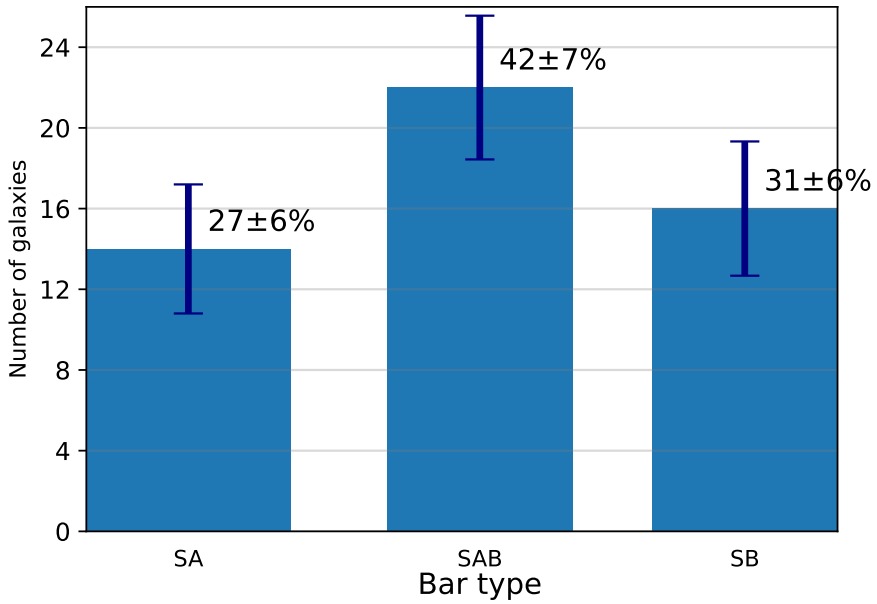

Figure 3: Bar distribution for our sample of galaxies. We have assigned an uncertainty for the percentage values assuming a binomial distribution.

catalogue. Other galaxies have been rejected even when present in the *HST* catalogue based on a perceived lack of clarity, on an insufficient coverage of the desired object or on the objects having been observed only in the UV and/or the NIR ranges. Because we left out known nuclear rings and because of the AINUR limitations, our sample is not not volume-complete.

In Fig. 3 we can see that our sample features a significant number of both barred and unbarred galaxies. In Fig. 4 we see that our sample consists mainly of galaxies with stellar masses between $10^{10}\,M_\odot$ and $10^{11}\,M_\odot$. Looking at Fig. 5 we notice that the vast majority of our galaxies are classified within the intermediate Hubble classes, between Sa and Sbc. These characteristics are innate to our sample and shall be taken into account during our analysis.

2.2 Sample

Our final working sample is composed of 52 galaxies with stellar or star-forming nuclear rings.

Most of the galaxies in AINUR, and hence in this work, are known to be barred. Twelve galaxies (NGC 2985, NGC 2997, NGC 4100, NGC 4459, NGC 4571, NGC 4736, NGC 4826, NGC 5033, NGC 6503, NGC 6753, NGC 7217 and NGC 7742) are not barred.

Three of the selected images were taken by the WFC3/UVIS, the ones for the galaxies NGC 1433, NGC 4459 and NGC 5728. Thirteen of them were taken using the ACS/WFC: NGC 1068, NGC 1097, NGC 1300, NGC 1566, NGC 1672, NGC 1808, NGC 2903, NGC 2985, NGC 4100, NGC 4800, NGC 5806, NGC 6503 and NGC 7469. The remaining of the used images were taken by the WFPC2.

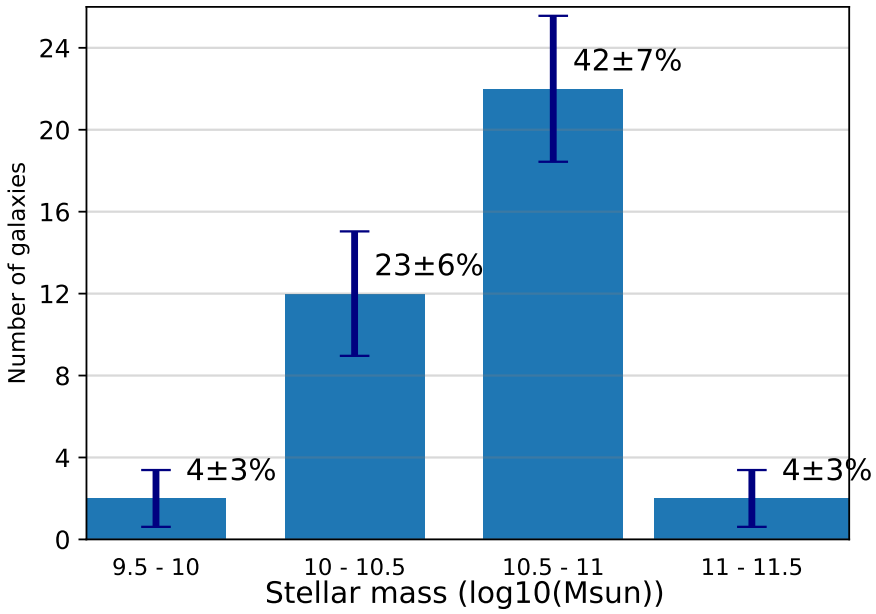

Figure 4: Stellar mass distribution for our sample of galaxies. We have assigned an uncertainty for the percentage values assuming a binomial distribution.

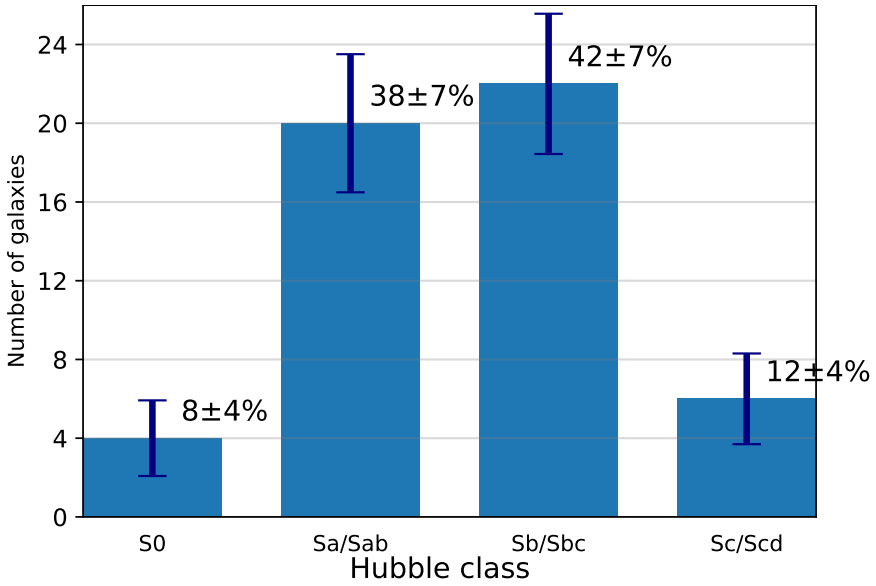

Figure 5: Hubble type distribution for our sample of galaxies. We have assigned an uncertainty for the percentage values assuming a binomial distribution.

Five of those exposures were taken with the *F606W* filter, for the galaxies: NGC 1241, NGC 3504, NGC 4593, NGC 5135 and NGC 5427. The one picturing NGC 4274 was taken with *F555W* and the one showing NGC 4321 was taken with *F702W*. The remaining galaxies were all pictured using the *F814W* filter.

ID	Distance (Mpc)	Morph. type	Instrument	Filter
NGC 278	11.7	SAB(rs)b	WFPC2	*F814W*
NGC 613	18.7	SB(rs)bc	WFPC2	*F814W*
NGC 864	21.8	SAB(rs)c	WFPC2	*F814W*
NGC 1068	15.3	(R)SA(rs)b	ACS/WFC	*F814W*
NGC 1097	15.2	(R′)SB(rs)b pec	ACS/WFC	*F814W*
NGC 1241	55.8	SAB(rs)b	WFPC2	*F606W*
NGC 1300	20.2	SB(rs)b	ACS/WFC	*F814W*
NGC 1317	23.9	(R′)SAB(rl)a	WFPC2	*F814W*
NGC 1326	16.1	(R_1)SAB(l)0/a	WFPC2	*F814W*
NGC 1433	11.6	(R′)SB(r)ab	WFC3/UVIS	*F814W*
NGC 1512	9.5	(R′)SB(r)ab pec	WFPC2	*F814W*
NGC 1566	17.4	(R′)SAB(s)bc	ACS/WFC	*F814W*
NGC 1672	15.0	(R:)SB(r)bc	ACS/WFC	*F814W*
NGC 1808	10.9	(R_1)SAB(s)b pec	ACS/WFC	*F814W*
NGC 2903	8.9	SAB(rs)bc	ACS/WFC	*F814W*
NGC 2985	22.6	(R′)SA(rs)ab	ACS/WFC	*F814W*
NGC 2997	13.1	SAB(s)c	WFPC2	*F814W*
NGC 3081	31.8	(RR)SAB(r)0/a	WFPC2	*F814W*
NGC 3185	18.9	(R)SB(r)a	WFPC2	*F814W*
NGC 3310	17.4	SA(rs)bc pec	WFPC2	*F814W*
NGC 3504	23.8	(R′)SAB(rs)ab	WFPC2	*F606W*
NGC 3982	23.6	SAB(r)b	WFPC2	*F814W*
NGC 4100 ⚠	18.6	(R′)SA(s)bc	ACS/WFC	*F814W*
NGC 4102	18.6	SAB(s)b?	WFPC2	*F814W*
NGC 4245	15.0	SB(r)0/a	WFPC2	*F814W*
NGC 4274	15.6	(R′)SB(r)ab	WFPC2	*F555W*
NGC 4303	23.1	SAB(rs)bc	WFPC2	*F814W*
NGC 4314	16.4	(R′)SB(R'_1)a	WFPC2	*F814W*
NGC 4321	24.0	SAB(s)bc	WFPC2	*F702W*
NGC 4448	11.7	(R)SB(r)ab	WFPC2	*F814W*
NGC 4459	16.1	SA(r)0^+	WFC3/UVIS	*F814W*
NGC 4571	16.8	SA(r)c	WFPC2	*F814W*
NGC 4593	35.3	(R′)SB(rs)ab	WFPC2	*F606W*
NGC 4736	5.2	(R)SAB(rs)ab	WFPC2	*F814W*
NGC 4800	14.5	SA(rs)b	ACS/WFC	*F814W*
NGC 4826 ⚠	7.5	(R′)SA(r)ab pec	WFPC2	*F814W*
NGC 5033 ⚠	15.4	SA(s)c	WFPC2	*F814W*
NGC 5135	57.4	SB(l)ab	WFPC2	*F606W*

ID	Distance (Mpc)	Morph. type	Instrument	Filter
NGC 5248	17.9	(R′)SAB(rs)bc	WFPC2	*F814W*
NGC 5427	39.4	SA(rs)bc	WFPC2	*F606W*
NGC 5728	39.7	(R_1)SAB(r)a	WFC3/UVIS	*F814W*
NGC 5806	20.5	SAB(s)b	ACS/WFC	*F814W*
NGC 6503	5.2	SA(s)cd	ACS/WFC	*F814W*
NGC 6753	41.8	(R)SA(r)b	WFPC2	*F814W*
NGC 6782	52.5	(RR)SB(r)a	WFPC2	*F814W*
NGC 6951	24.4	SAB(rs)bc	WFPC2	*F814W*
NGC 7217	16.0	(R)SA(r)ab	WFPC2	*F814W*
NGC 7469	70.7	(R′)SAB(rs)a	ACS/WFC	*F814W*
NGC 7552	20.2	(R′)SB(s)ab	WFPC2	*F814W*
NGC 7742	24.2	SA(r)ab	WFPC2	*F814W*
ESO 565-11	66.5	(R′)SB(rs)a	WFPC2	*F814W*
IC 342	3.3	SAB(rs)cd	WFPC2	*F814W*

Table 1: Identification (col. 1), Distance (col. 2, from AINUR (Comerón et al. 2010)), morphological type (col. 3, from Buta et al. (2007) when available and from NED for the other galaxies), instrument and filter from *HST* used to take the used image (col. 4 and col. 5). A warning sign (⚠) appears besides very inclined galaxies.

3 Image Processing

Once we have selected a *HST* image with a good view of the galaxy centre, we looked for methods of image processing in order to enhance the inner structure of the pictured galaxy.

We considered two different methods: unsharp-masking (Malin 1977; Schweizer & Ford 1985) and structure maps (Pogge & Martini 2002). The first one, unsharp-masking, is achieved with a convolution of the image and a Gaussian kernel followed by a division. The latter uses the PSF of the instrument to create, through a convolution a smoothed version of the original image that is then used as divisor with the original as dividend, the result goes through one final convolution with the transpose of the PSF to create the so-called structure map.

After testing and comparing both methods (Fig. 6), we settled with unsharp-masking for our work. This approach has been demonstrated to yield comparable outcomes to those achieved through the use of structure maps, while offering enhanced speed, versatility, and convenience. This is due to the facts that the instrument PSF is not a required input, that we are allowed to change the width of the Gaussian kernel and that less operations are necessary.

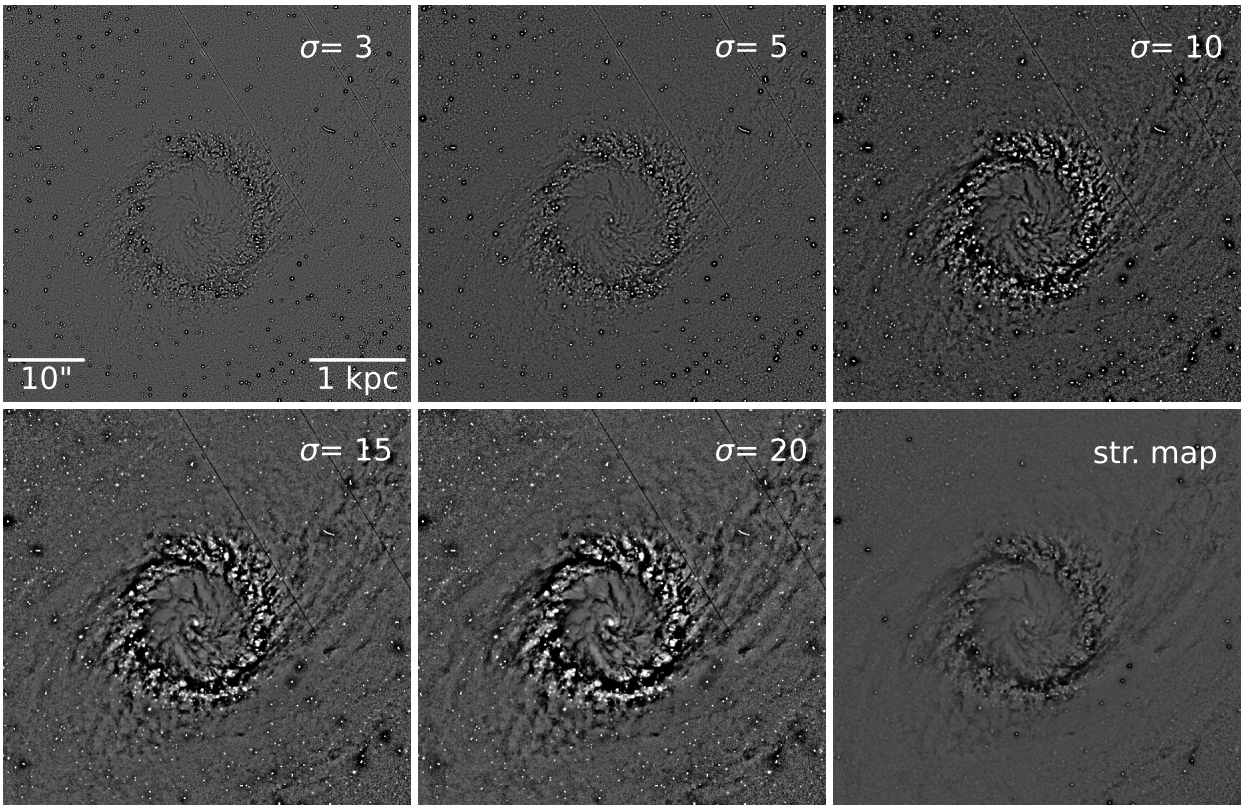

Figure 6: For our test we used an image of NGC 1097 with the *F814W* filter taken with the ACS/WFC. In the upper row: the resultant unsharp-masked image for a Gaussian kernel with a sigma of 3, 5 and 10 pixels respectively. In the lower row, from left to right: the resultant unsharp-masked image for a Gaussian kernel with a cross-section of 15 and 20 pixels and the outcome of the structure map technique.

3.1 Unsharp-masking

This technique is essentially used to uncover small scale variations in the structure under the larger brightness distribution. To achieve this, first the original CCD image is convolved with a Gaussian kernel, the original image is then divided by the resultant smoothed image, so to obtain an unsharp-masked image.

$$I_{UM} = \frac{I_0}{I_0 * G}. \tag{1}$$

This method was taken from Heisler & Vader (1994), and was first used by Malin (1977) and Schweizer & Ford (1985). The Gaussian kernels used by Heisler & Vader (1994) had sigmas of 3 to 10 pixels, however, after performing some tests (Fig. 6) and considering the significantly higher angular resolution of our images compared to those used by Heisler & Vader (1994), we concluded that we needed to use larger kernels, with sigmas between 10 and 30 pixels in order to discern the internal dust structure of the galaxies in the sample. For most galaxies, we used a sigma of 20 pixels, except for NGC 864, NGC 1433 and NGC 4571 for which we used a sigma of 30 pixels and NGC 1097, NGC 4593 and NGC 5135 for which we used a sigma of 15 pixels. A method with similar basis and principles, applied to study *HST* data can be found in Elmegreen et al. (2002).

The result is an image where the dust structure is visible, both the most external one that already was visible and the one closer to the centre, that was previously obscured by the light. This method does not reveal any structure that was not already present in the *HST* image, but rather brings it to the forefront and makes it easier to observe and characterise.

4 Sample classification

We have grouped the galaxies into different classes within three different visual classifications, two of them are based on the galaxy morphology and the last one is based on the ring morphology.

In the interest of properly classifying the galaxies on their morphology we have used S^4G (Spitzer Survey of Stellar Structure in Galaxies; Sheth et al. 2010) images when available, and specially when the *HST* image is not large enough to view the full scope of the galaxy. The S^4G is a survey of 2331 galaxies using the Infrared Array Camera (IRAC) installed in the *Spitzer Space Telescope* at 3.6 and 4.5μm.

In addition, another classification was made on the basis of the presence of distinguishable nuclear features, mainly nuclear spirals, within the inside of the ring.

4.1 Galaxy morphology classification

This classification is focused on the visual structure of the galaxy as a whole, the three types are: Flocculent, Multi-armed and Grand Design galaxies. These classes are based on the work from Elmegreen & Elmegreen (1985), and the classification has been carried out using the work of Elmegreen et al. (2011) as reference.

Flocculent galaxies are characterised by a sort of chaotic structure without any arm dominating over the rest, but rather a fragmented and interlaced dust spiral towards the centre with very short armlets, like NGC 4459.

Multi-armed galaxies have various long and continous prevalent arms, like NGC 3982.

Finally, **Grand Design** galaxies have a better defined structure, composed of a clear core and two long well-defined arms that circle around it, like NGC 4314.

Examples of these classes can be seen in Fig. 7.

4.2 Spiral structure compactness classification

For this work we have created a new morphological classification, in the same vein as the classical Hubble sequence classification. It consists of a visual categorisation of galaxies, attending to the arm structure, mainly arm density, around the nuclear ring and how open said structure is.

Some examples are: NGC 278 as one of the most compact galaxies, NGC 1300 as one of the least compact and NGC 1241, that lies in between (Fig. 8).

4.3 Nuclear ring classification

This classification concentrates on the structure that surrounds the nuclear ring and in the dust lanes that reach it. The different kinds of nuclear ring structure that we have selected are:

two-armed, 2 armed with additional paths and many-armed.

two-armed: The nuclear rings of these galaxies are surrounded by mostly empty space except for two symmetric dust lanes that get to them.

2 armed with additional paths (2arms+): These galaxies present a nuclear ring crowded with dust lanes among which two stand out as more prevalent.

many-armed: This category includes galaxies in which the nuclear ring is fed by various, similar arms, with no recognisable hierarchy, like NGC 6753.

The two-armed and 2 arms+ categories may seem similar, as both are characterised by the dominance of two symmetric arms that lead to the nuclear ring. The difference between these two classes resides in the presence of smaller armlets, apart of the two main arms, around the nuclear ring. For example, NGC 7552 (2 arms+) opposite to NGC 1512 (two-armed), we can see that NGC 7552 presents more structure, with dust following paths outside the direction of the two main arms, while the nuclear region of NGC 1512 is nearly free of dust outside of the said two main arms.

Examples of these categories can be seen in Fig. 9.

4.4 Nuclear spirals

After applying the unsharp-masking to our sample we noticed the presence of nuclear spirals inside some of the rings. These configurations correspond to dust lanes that seem to arise from the nuclear ring, sometimes even beyond the nuclear ring, and extend up to the very centre following a spiral morphology.

Of the 32 galaxies for which we were able to study the inside of the nuclear ring using *HST* images, we have observed nuclear spirals in 28 of the galaxies in our sample: NGC 1068, NGC 1097, NGC 1300, NGC 1317, NGC 1326, NGC 1433, NGC 1512, NGC 1566, NGC 1672, NGC 2997, NGC 3081, NGC 3504, NGC 3982, NGC 4303, NGC 4314, NGC 4321, NGC 4593, NGC 4736, NGC 4800, NGC 5033, NGC 5248, NGC 5728, NGC 5806, NGC 6753, NGC 6782, NGC 6951, NGC 7469 and NGC 7742. The rest of the sample either does not showcase this structure (like ESO 565-11) or the angular resolution and the overall visibility of the nuclear region is not good enough to properly determine whether nuclear spirals are present or not (like NGC 3185), as seen in Fig. 10.

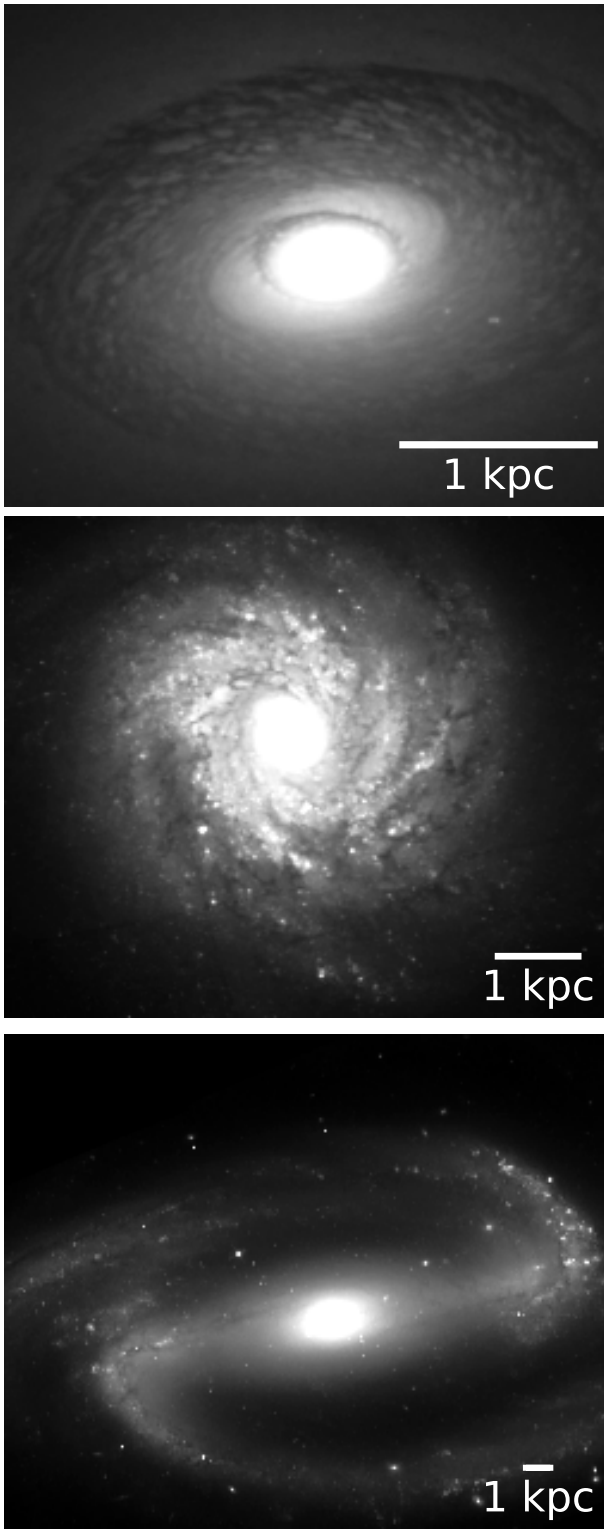

Figure 7: Morphology classification examples. From top to bottom: NGC 4459 (Flocculent), NGC 3982 (Multi-armed) and NGC 1300 (Grand Design)

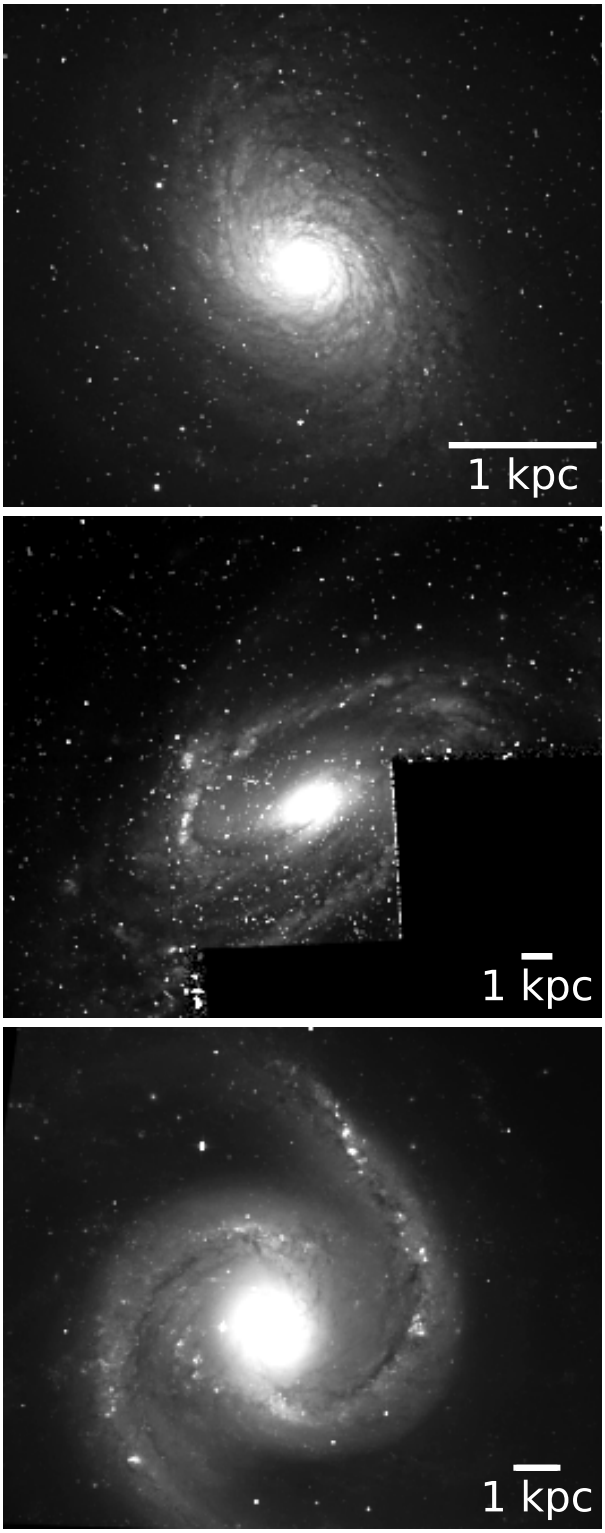

Figure 8: Spiral compactness classification examples. From top to bottom and from most to least compact: NGC 4800, NGC 1241 and NGC 1566

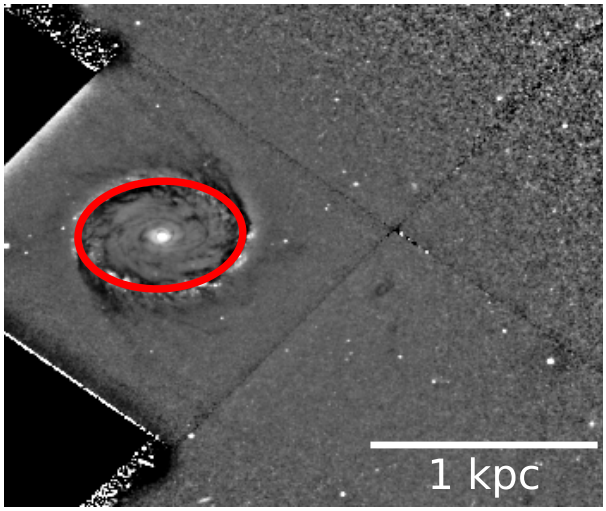

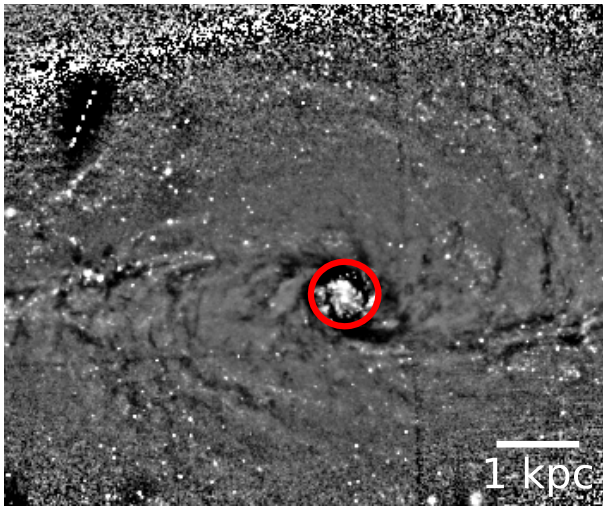

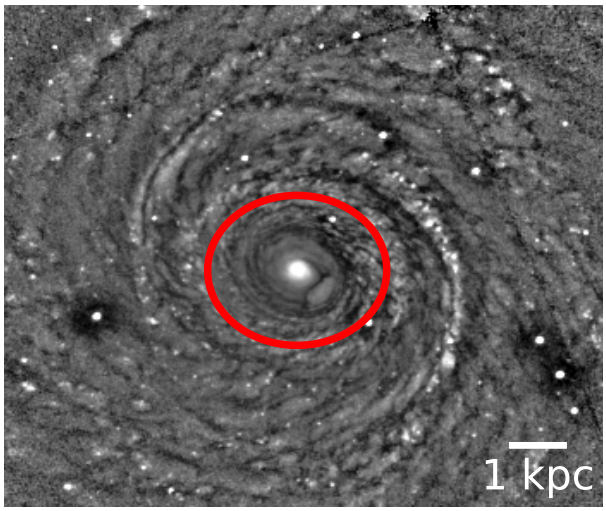

Figure 9: Ring classes examples. From top to bottom: NGC 1512 (two-armed), NGC 7552 (2 arms+) and NGC 6753 (many-armed)

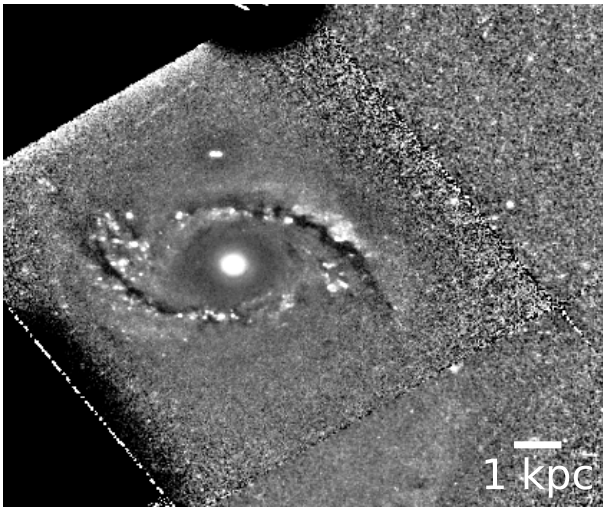

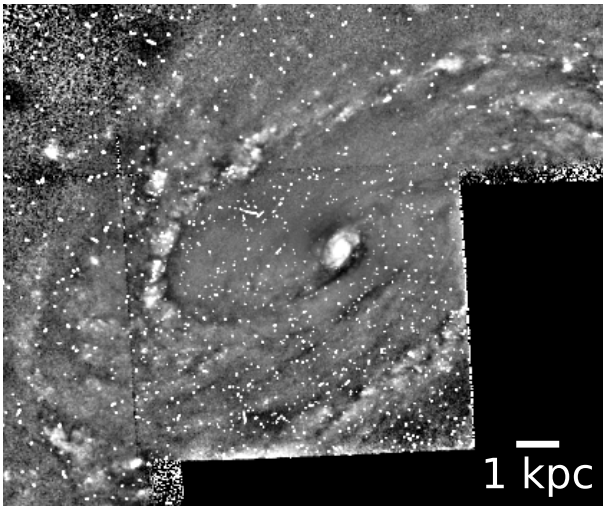

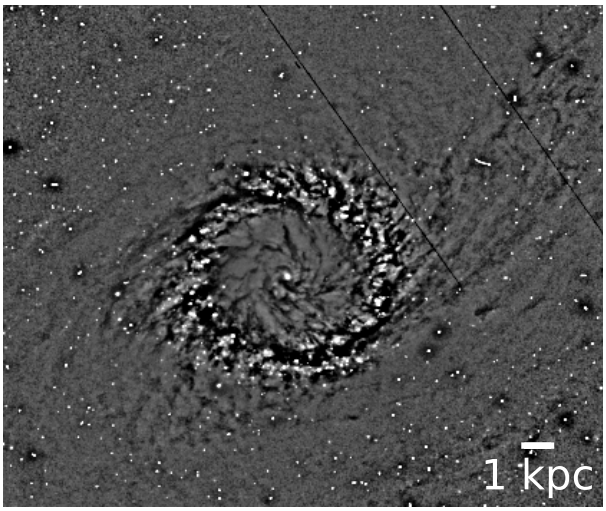

Figure 10: Examples of nuclear features. From top to bottom: ESO 565-11, with no discernible nuclear features; NGC 1241 for which the angular resolution does not allow us to distinguish any nuclear features and NGC 1097 featuring a nuclear spiral.

ID	Bar type	Morph. class	Ring class	Comp.	Nuclear spiral	$\log(M_*$ / $\mathrm{M}_\odot)$
NGC 278	SAB	F	many-armed	Most	?	-
NGC 613	SB	GD	2 arms+	Inter.	?	11.087
NGC 864	SAB	M	2 arms+	Inter.	?	10.184
NGC 1068	SA	M	2 arms+	Inter.	✓	10.861
NGC 1097	SB	GD	2 arms+	Least	✓	11.24
NGC 1241	SAB	M	2 arms+	Inter.	?	-
NGC 1300	SB	GD	two-armed	Least	✓	10.576
NGC 1317	SAB	F	two-armed	Inter.	✓	-
NGC 1326	SAB	GD	two-armed	Least	✓	10.551
NGC 1433	SB	GD	two-armed	Least	✓	10.297
NGC 1512	SB	GD	two-armed	Least	✓	10.333
NGC 1566	SAB	GD	two-armed	Least	✓	10.584
NGC 1672	SB	GD	2 arms+	Least	✓	10.661
NGC 1808	SAB	F	many-armed	Inter.	?	10.615
NGC 2903	SAB	GD	many-armed	Inter.	?	10.665
NGC 2985	SA	F	many-armed	Most	?	10.856
NGC 2997	SAB	M	2 arms+	Inter.	✓	-
NGC 3081	SAB	GD	2 arms+	Least	✓	-
NGC 3185	SB	GD	2 arms+	Most	?	10.215
NGC 3310	SA	M	2 arms+	Inter.	?	10.319
NGC 3504	SAB	GD	2 arms+	Inter.	✓	10.404
NGC 3982	SAB	M	many-armed	Most	✓	10.258
NGC 4100 ⚠	SA	M	many-armed	Most	?	10.576
NGC 4102	SAB	M	many-armed	Inter.	?	10.554
NGC 4245	SB	GD	two-armed	Least	×	9.801
NGC 4274	SB	F	many-armed	Most	?	10.759
NGC 4303	SAB	M	2 arms+	Least	✓	10.857
NGC 4314	SB	GD	two-armed	Least	✓	10.14
NGC 4321	SAB	GD	2 arms+	Least	✓	10.931
NGC 4448	SB	F	2 arms+	Least	?	10.848
NGC 4459	SA	F	2 arms+	Most	×	-
NGC 4571	SA	M	many-armed	Inter.	?	10.254
NGC 4593	SB	GD	two-armed	Least	✓	10.932

ID	Bar type	Morph. class	Ring class	Comp.	Nuclear spiral	$\log(M_*/\mathrm{M}_\odot)$
NGC 4736	SAB	GD	many-armed	Inter.	✓	10.521
NGC 4800	SA	M	many-armed	Most	✓	10.463
NGC 4826 ⚠	SA	F	many-armed	Most	?	10.443
NGC 5033 ⚠	SA	M	many-armed	Most	✓	10.946
NGC 5135	SB	GD	two-armed	Least	?	-
NGC 5248	SAB	GD	2 arms+	Inter.	✓	10.673
NGC 5427	SA	M	2 arms+	Inter.	?	10.737
NGC 5728	SAB	GD	2 arms+	Least	✓	10.849
NGC 5806	SAB	M	2 arms+	Inter.	✓	10.585
NGC 6503	SA	F	many-armed	Most	?	9.697
NGC 6753	SA	M	many-armed	Most	✓	-
NGC 6782	SB	GD	two-armed	Least	✓	-
NGC 6951	SAB	GD	two-armed	Least	✓	-
NGC 7217	SA	F	many-armed	Most	×	-
NGC 7469	SAB	M	2 arms+	Inter.	✓	-
NGC 7552	SB	GD	2 arms+	Least	?	10.523
NGC 7742	SA	F	many-armed	Most	✓	10.343
ESO 565-11	SB	GD	two-armed	Least	×	-
IC 342	SAB	M	2 arms+	Inter.	?	-

Table 2: Identification (col. 1), bar type (col. 2, from Buta et al. (2007) when available and from NED for the other galaxies), morphology class (col. 3, GD for Grand Design, M for Multiarm and F for Flocculent), ring morphology class (col. 4), spiral compactness class (col. 5, Most for most compact, Least for least compact and Inter. for the galaxies that lie in between), nuclear spiral (col. 6, ✓ if the galaxy exhibits a nuclear spiral, × if it does not and ? if the image does not allow for an answer) and stellar mass (col. 7, from Sheth et al. (2010) when available). A warning sign (⚠) appears besides very inclined galaxies for which the classification might be uncertain.

5 Results

We have concluded that the morphological distribution of our sample is: 24 Grand Design galaxies, 17 Multi-armed galaxies and 11 Flocculent. Therefore our sample is slightly biased towards Grand Design galaxies, but we do obtain a considerable amount for each type.

Regarding our compactness classification, we have selected 14 galaxies as part of the most compact type, 20 galaxies as part of the least compact type and 18 lying in between.

The ring type classification resulted in a distribution of 13 galaxies with rings that only show two dust lanes, 22 galaxies with two main dust lanes and additional smaller ones and 17 galaxies presenting many arms leading into the ring.

The nuclear features classification resulted in a group of 28 galaxies featuring nuclear spirals, 6 galaxies with no nuclear features and 18 galaxies for which we can not properly study the galaxy centre.

Following this process, we proceeded to cross-reference these classifications with themselves and with known galaxy characteristics to highlight and find tendencies and predispositions in the ring formation within these galaxies.

5.1 Ring classes distribution

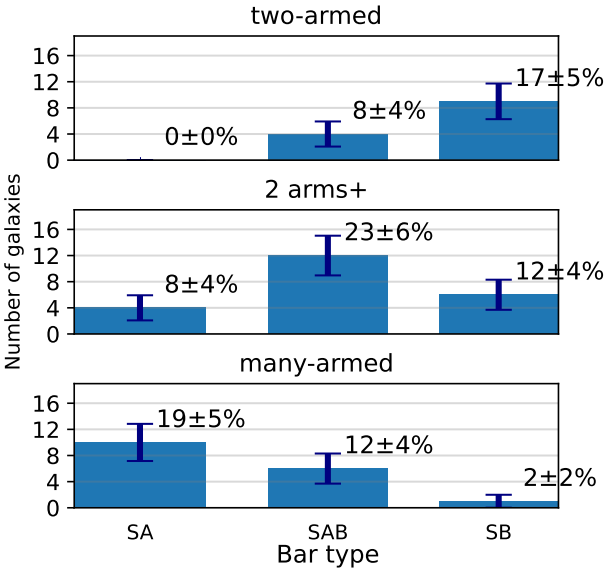

Figure 11: Bar distribution for each ring type, indicating the percentage of the total represented by each combination. We have assigned an uncertainty for the percentage values assuming a binomial distribution.

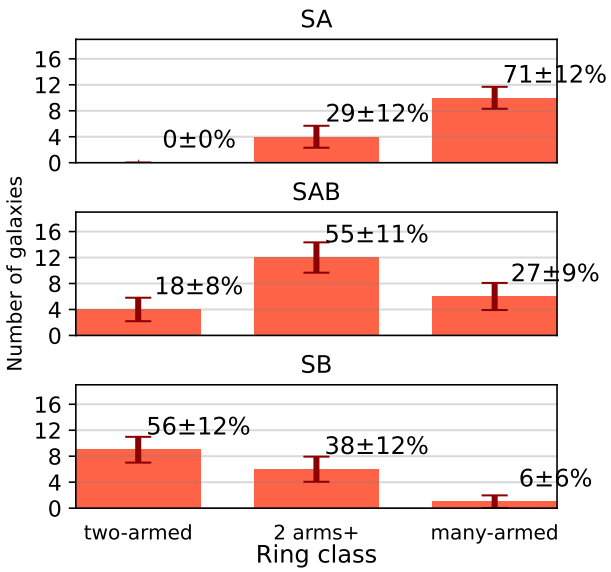

Figure 12: Ring class distribution for each bar type, indicating the percentage of the galaxies in each bar type that present each ring class. We have assigned an uncertainty for the percentage values assuming a binomial distribution.

As seen in Fig. 11, Fig. 13, Fig. 15, Fig. 17 and Fig. 20, we have extracted the bar, Hubble type, stellar mass, morphological and compactness distributions for each of the ring classes we have previously defined. The percentage of the total represented by each combination is shown. For these and all subsequent histograms we have assigned an uncertainty for the percentage values assuming a binomial distribution.

In Fig. 12, Fig. 14, Fig. 16, Fig. 18 and Fig. 19, we present the ring classes distributions for each of the bar, Hubble type, stellar mass, morphological and compactness types. The percentage of galaxies in each type that showcase each ring class is shown.

In Fig. 11 and Fig. 12 we observe that two-armed rings appear in either barred or weakly barred galaxies exclusively, while the 2 arms+ rings can appear in non-barred galaxies, but do mostly in weakly barred ones. The many-armed rings seem to emerge indistinctly in both non and weakly barred galaxies whereas they are very uncommon in strongly barred ones. We can distinguish a pattern in which each ring class, from two-armed to many-armed rings, has a diminishing affinity towards bars.

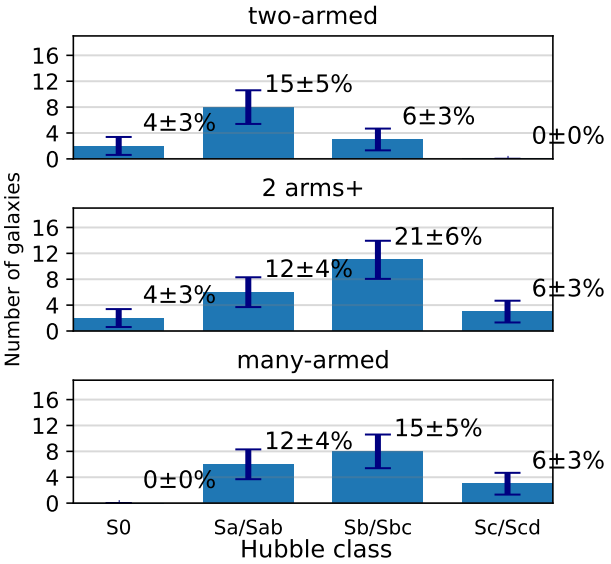

Figure 13: Hubble type distribution for every ring type. We have assigned an uncertainty for the percentage values assuming a binomial distribution.

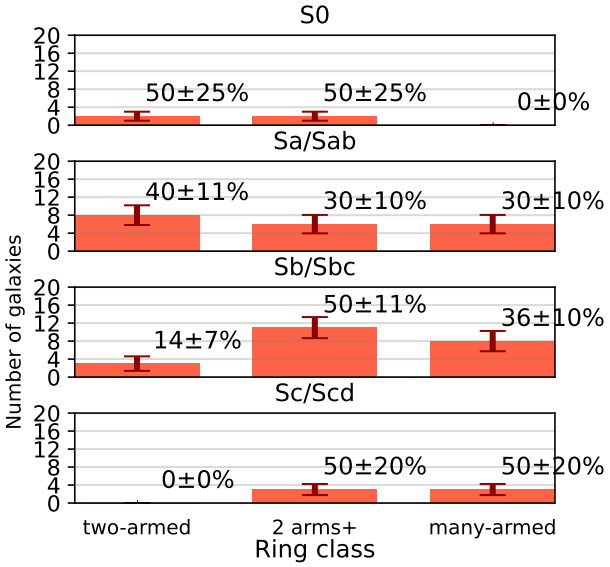

Figure 14: Ring class distribution for each Hubble type, indicating the percentage of the galaxies in each Hubble type that present each ring class. We have assigned an uncertainty for the percentage values assuming a binomial distribution.

Figures 13 and 14 highlight that two-armed rings appear mostly in earlier Hubble classes, such as Sa or Sab. 2 arms+ rings and many-armed rings are much more present in later Sb or Sbc classes.

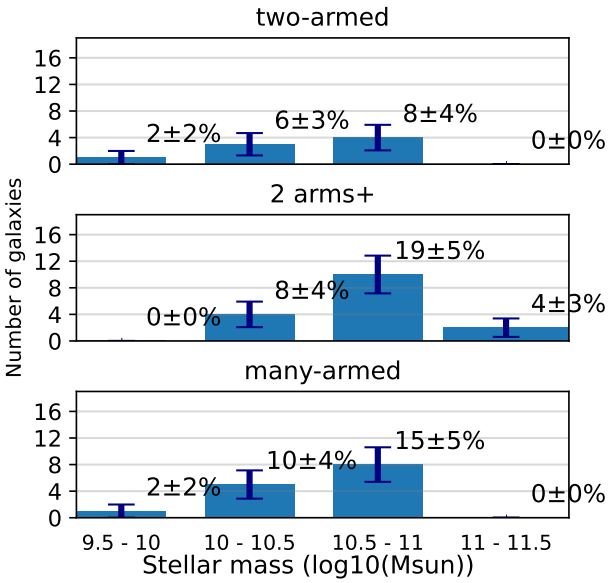

Figure 15: Stellar mass distribution for every ring type. We have assigned an uncertainty for the percentage values assuming a binomial distribution.

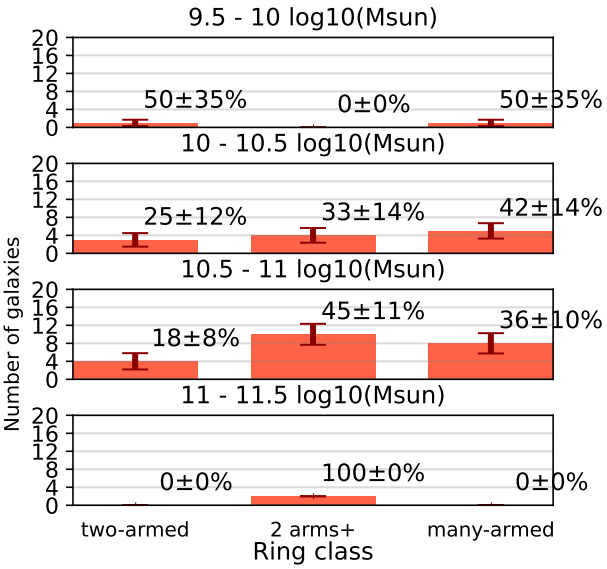

Figure 16: Ring class distribution for each stellar mass range, indicating the percentage of the galaxies in each mass range that present each ring class. We have assigned an uncertainty for the percentage values assuming a binomial distribution.

In Fig. 15 we see that the stellar mass distribution for each ring class is very similar to that shown in Fig 4. In Fig. 16 we see that the histograms are almost flat, suggesting that there is no relation between ring classes and stellar mass.

In Fig. 17 and Fig. 18 we see that the two-armed rings are plentifully observed in Grand Design galaxies. They are present in half of the Grand Design galaxies in our sample, and extremely infrequent in the other classes and almost a quarter of our sample is made up of this combination (Grand Design galaxy with two-armed ring) of galaxy and ring types. Similarly to the two-armed rings, 2 arms+ rings are very difficult to find in Flocculent galaxies, but are very common in Grand Design and Multiarmed galaxies. Finally, many-armed rings elude Grand Design galaxies and are observed in more than 70 % of Flocculent galaxies. The overall pattern of this distribution shows that histograms corresponding to each ring class and to each morphological type gradually skew from showcasing a relation between Grand design galaxies and two-armed rings to showcasing one between Flocculent galaxies and many-armed rings.

In Figures 19 and 20 we observe that two-armed rings prevail in the least compact galaxies, 2 arms+ do so for the intermediate cases and many-armed rings dominate in the most compact galaxies.

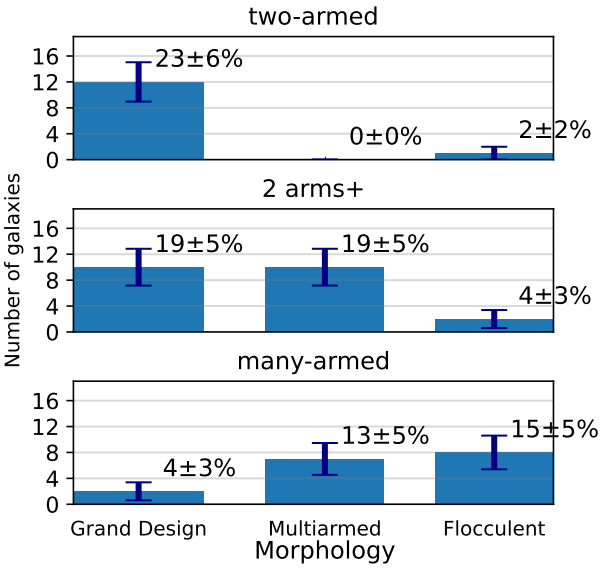

Figure 17: Morphology distribution for every ring type. We have assigned an uncertainty for the percentage values assuming a binomial distribution.

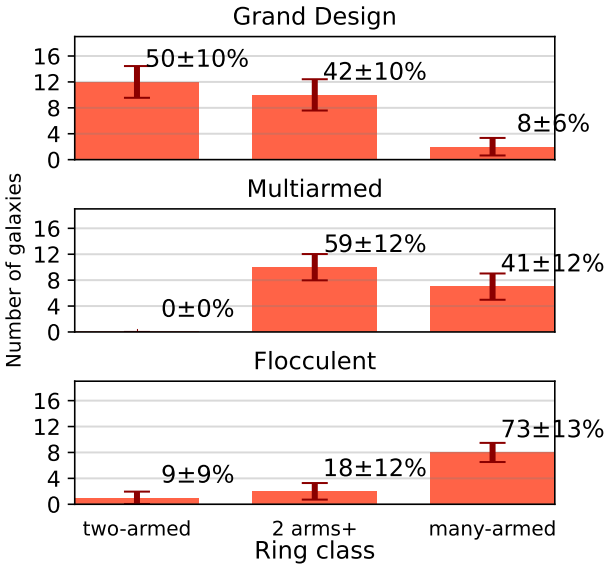

Figure 18: Ring class distribution for each morphology class, indicating the percentage of the galaxies in each morphology class that present each ring class. We have assigned an uncertainty for the percentage values assuming a binomial distribution.

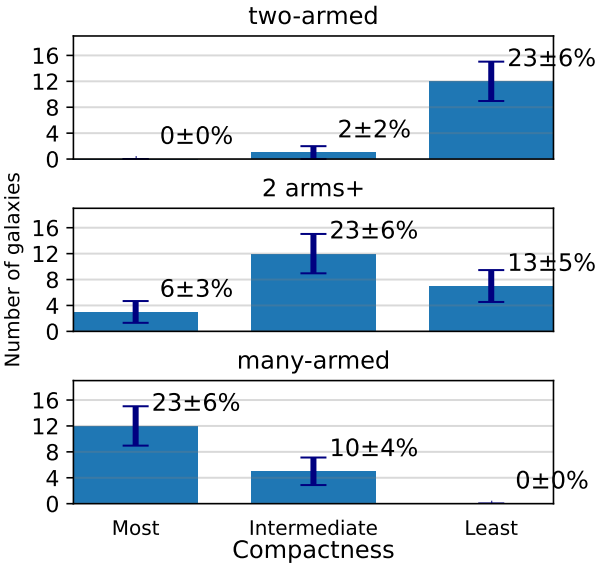

Figure 19: Spiral compactness distribution for every ring type. "Most" stands for most compact, "Least" for least compact and "Intermediate" for in-between cases. We have assigned an uncertainty for the percentage values assuming a binomial distribution.

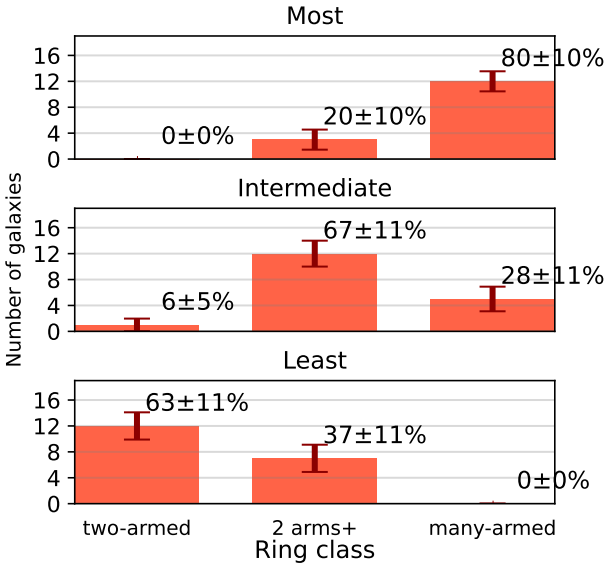

Figure 20: Ring class distribution for each spiral compactness class, indicating the percentage of the galaxies in each class that present each ring class. "Most" stands for most compact, "Least" for least compact and "Intermediate" for in-between cases. We have assigned an uncertainty for the percentage values assuming a binomial distribution.

5.2 Nuclear spirals

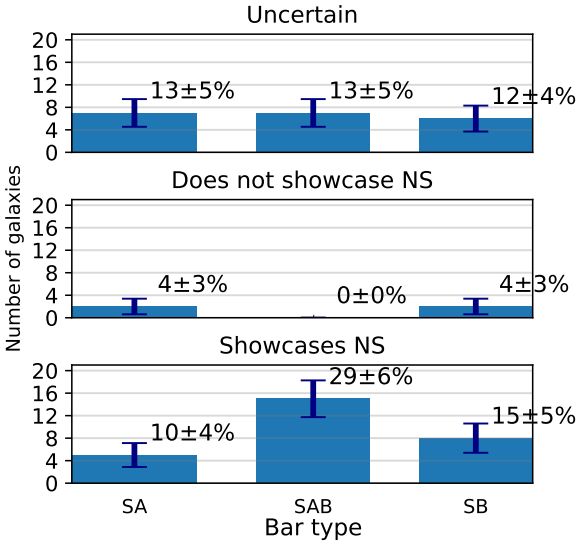

Figure 21: Bar distribution for galaxies featuring nuclear spirals. We have assigned an uncertainty for the percentage values assuming a binomial distribution.

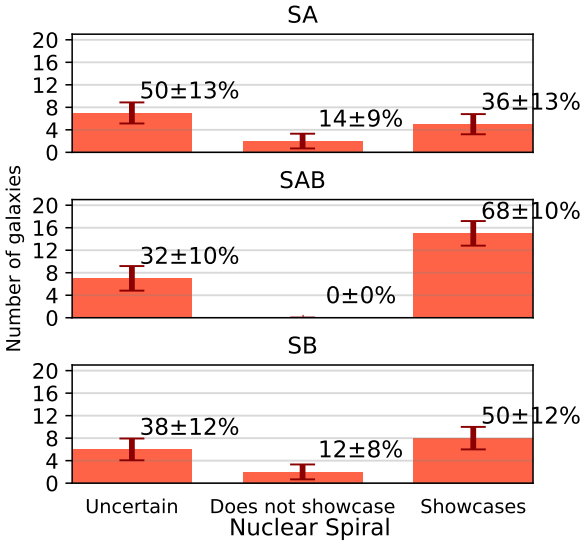

Figure 22: Distribution of nuclear spirals for each bar type, indicating the percentage of the galaxies in each bar type that either showcase nuclear spirals ("Showcase"), do not ("Do not showcase") or it is uncertain ("Uncertain"). We have assigned an uncertainty for the percentage values assuming a binomial distribution.

We can only be sure that there is no nuclear spiral in 4 galaxies, we have found them in more than half of our complete sample. They are present in almost all galaxy types. This suggests that nuclear spirals are a common phenomenon in galaxies featuring nuclear rings.

The vast majority of galaxies where we have detected a nuclear spiral are barred (as shown in Figs. 21 and 22), Grand Design (as shown in Figs. 23 and 24) and have the least compact spiral arms (as shown in Figs. 25 and 26).

When we checked our subsample of nuclear spirals against our own ring classification, as seen in Figs. 27 and 28. We notice that nuclear spirals are very common in galaxies featuring two-armed nuclear rings, and very rare in the ones that feature many-armed rings.

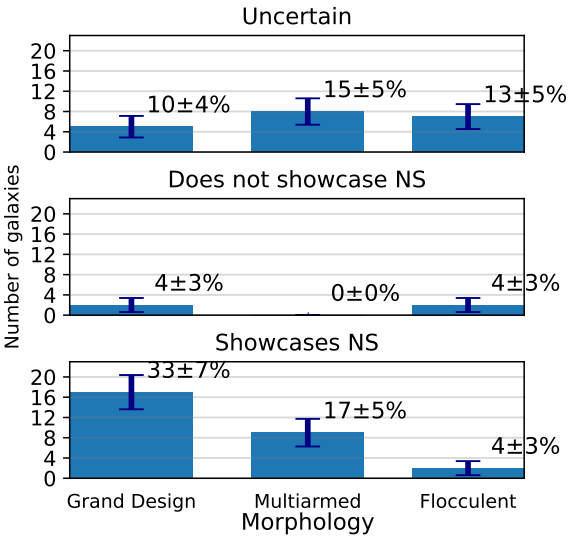

Figure 23: Morphology distribution for galaxies showcasing nuclear spirals("Showcases NS"), not ("Do not showcase NS") or it is uncertain ("Uncertain"). We have assigned an uncertainty for the percentage values assuming a binomial distribution.

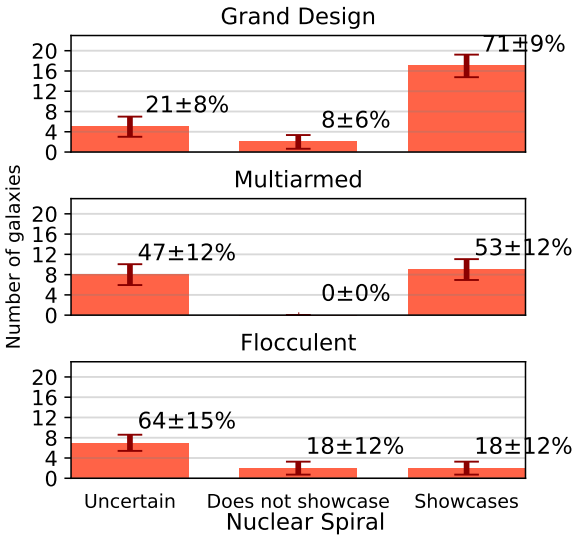

Figure 24: Distribution of nuclear spirals for each morphology class, indicating the percentage of the galaxies in each class that either showcase nuclear spirals ("Showcase"), do not ("Do not showcase") or it is uncertain ("Uncertain"). We have assigned an uncertainty for the percentage values assuming a binomial distribution.

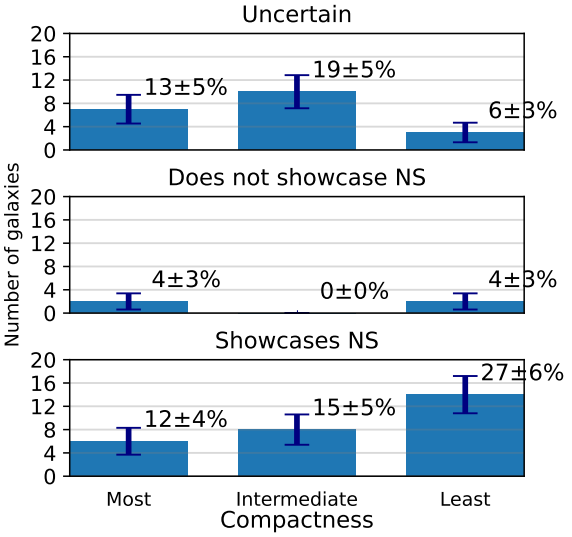

Figure 25: Compactness distribution for galaxies showcasing nuclear spirals("Showcases NS"), not ("Do not showcase NS") or it is uncertain ("Uncertain"). We have assigned an uncertainty for the percentage values assuming a binomial distribution. "Most" stands for most compact, "Least" for least compact and "Intermediate" for in-between cases.

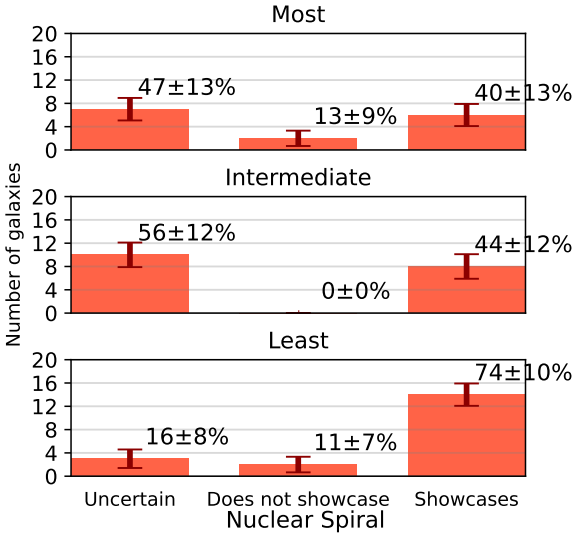

Figure 26: Distribution of nuclear spirals for each spiral compactness class, indicating the percentage of the galaxies in each class that either showcase nuclear spirals ("Showcase"), do not ("Do not showcase") or it is uncertain ("Uncertain"). "Most" stands for most compact, "Least" for least compact and "Intermediate" for in-between cases. We have assigned an uncertainty for the percentage values assuming a binomial distribution.

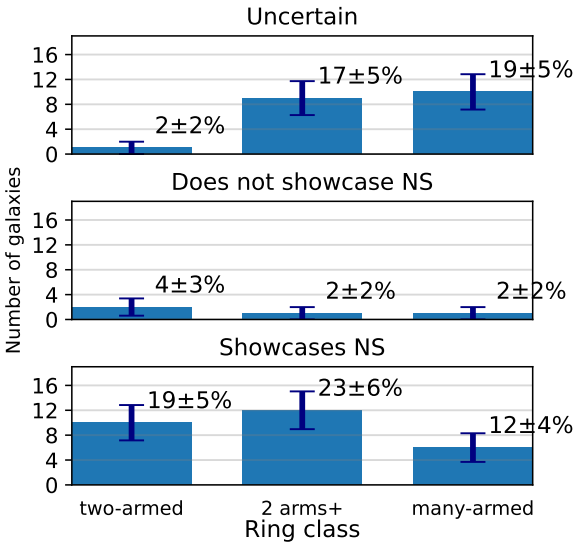

Figure 27: Ring class distribution for galaxies showcasing nuclear spirals("Showcases NS"), not ("Do not showcase NS") or it is uncertain ("Uncertain"). We have assigned an uncertainty for the percentage values assuming a binomial distribution.

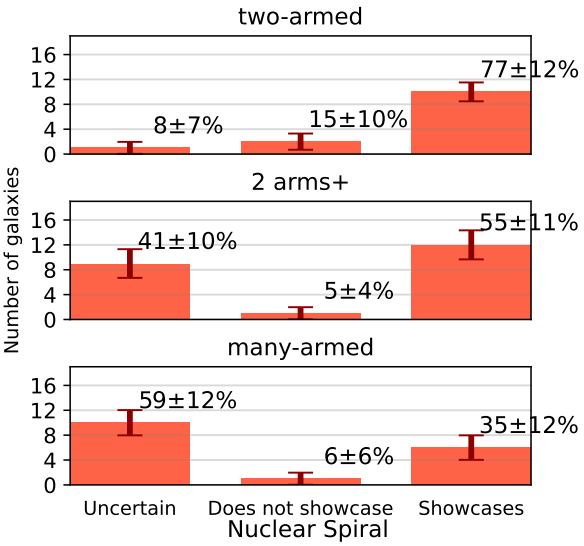

Figure 28: Distribution of nuclear spirals for each ring class, indicating the percentage of the galaxies in each class that either showcase nuclear spirals ("Showcase"), do not ("Do not showcase") or it is uncertain ("Uncertain"). We have assigned an uncertainty for the percentage values assuming a binomial distribution.

5.3 Discussion

5.3.1 Nuclear rings

5.3.1.1 Morphological relations

The histograms presented in Figs. 11 and 12 (bar type distribution), 13 and 14 (Hubble type distribution) and 17 and 18 (morphology distribution) show a common trend, with a gradual variation of the histogram skewness towards different ring classes. In Fig. 11, we see that two-armed rings prefer SB galaxies while many-armed rings prefer SA galaxies. In Fig. 17, we see that two-armed rings prefer Grand Design galaxies while many-armed rings prefer Multiarmed galaxies. In Fig. 13, the trend is similar, two-armed rings prefer earlier stages like Sa or Sab while many-armed rings prefer later stages like Sb and Sbc.

The fact that we found these similar trends in the distributions of the morphological properties is due to these properties not being independent. According to Elmegreen & Elmegreen (1985), a connection exists between the size and strength of bars and the Hubble type of the host galaxy, resulting in stronger bars for earlier type galaxies and weaker or absent bars for later type galaxies. And according to Elmegreen & Elmegreen (1989), earlier type galaxies are classified as Grand Design more often while later type galaxies are classified as Multi-armed and Flocculent. Combining

these results we can conclude that Grand Design galaxies tend to be strongly barred and earlier in type, Multi-armed galaxies usually present weaker bars and are of later type and lastly Flocculent galaxies are generally later type and feature even weaker bars or none at all.

Our statistical sample of 52 galaxies with nuclear rings demonstrates the following relations between the previously discussed morphological properties of the host and the morphology of the nuclear ring itself:

- **two-armed** rings appear more frequently in earlier type Grand design strongly barred galaxies with the least compact nuclear arm structures.

- **2 arms+** rings are observed more often in later type weakly barred galaxies, both Grand Design and Multiarmed.

- **many-armed** rings are more frequent in later type non-barred Flocculent and Multiarmed galaxies with a compact nuclear arm structure.

	ϵ_b	Q_g
two-armed	0.56	0.293
2 arms+	0.49	0.237
many-armed	0.38	0.159

Table 3: Average values of the maximum ellipticity of the bar ϵ_b and the non-axisymmetric torque parameter Q_g (from Comerón et al. 2010) for each ring class.

In Table 3 we can see the average values, taken from AINUR, of the maximum ellipticity of the bar ϵ_b and the non-axisymmetric torque parameter Q_g, that measures the impact of non-axisymmetries in the galaxy (Combes & Sanders 1981). These two parameters serve to get an idea of the bar strength, the stronger the bar, the higher Q_g and ϵ_b. We see that galaxies hosting two-armed rings present the strongest bars, the ones that host 2 arms+ rings have slightly weaker bars and many-armed rings appear in galaxies with very weak nonaxisymmetries.

The conclusion is that the morphology of the host galaxy, and more precisely the presence and properties of a bar play a fundamental role in determining the morphology of the nuclear ring and the nuclear region.

5.3.1.2 Notes on the dynamical explanation of nuclear rings formation

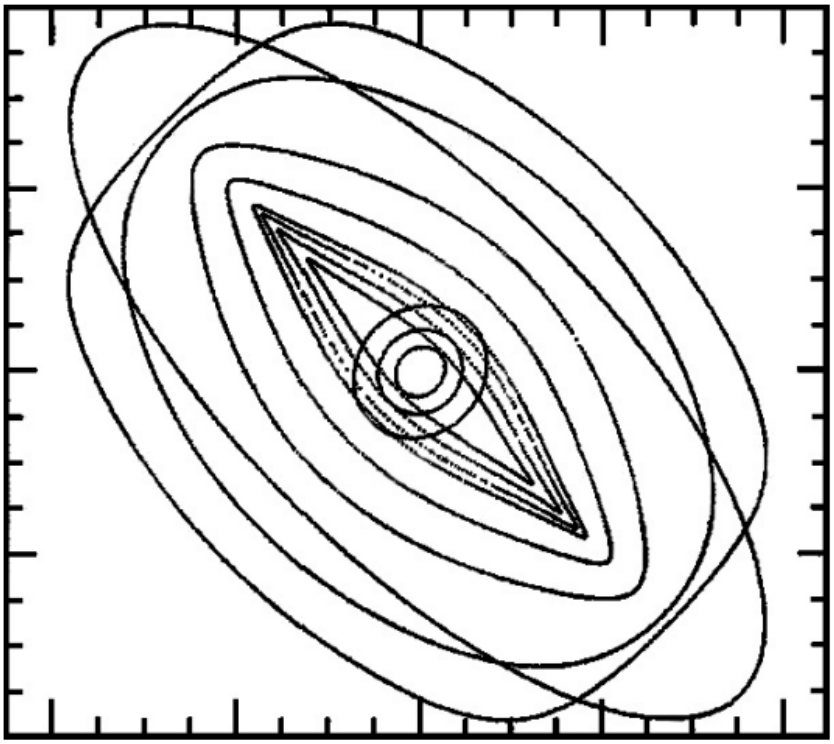

Figure 29: From Englmaier & Gerhard (1997), examples of the principal orbit families for a bar oriented at 45º. The elongated orbits parallel to the bar are the x_1 family, out of which the bar is constructed. Inside the ILR (or the outer ILR, if there are two LRs), the x_2 family is perpendicular to the bar.

The kinematic explanation for the origin of star formation nuclear rings in barred galaxies has previously been discussed in the literature. In Zurita et al. (2004), their study of CO kinematics in the barred Grand Design galaxy NGC 1530 improves over the previous work by Reynaud & Downes (1998), examining their hypothesis that strong velocity changes inhibits star formation, and how that explains why CO is observed all along the galaxy, yet star formation is mainly enhanced at the centre of the bar. Gas particles in strong bars can get trapped in looping orbits that can produce collisions, that end up in a shock that takes place in the far end of the bar and traps the clumps of gas into a dust lane (see Fig. 30) following an elongated orbit, aligned with the bar, falling into a much more circular x_2 orbit near the nucleus and between the ILRs (see Fig. 29). Therefore, the gas accumulates in x_2 orbits forming a ring and, if the density gets high enough, igniting star formation. Two-armed rings, present in strongly-barred galaxies, show signs of following this process, featuring a 180º symmetry forced by the bar potential. The two main dust lanes correspond to the shocked gas falling towards circumnuclear x_2 orbits.

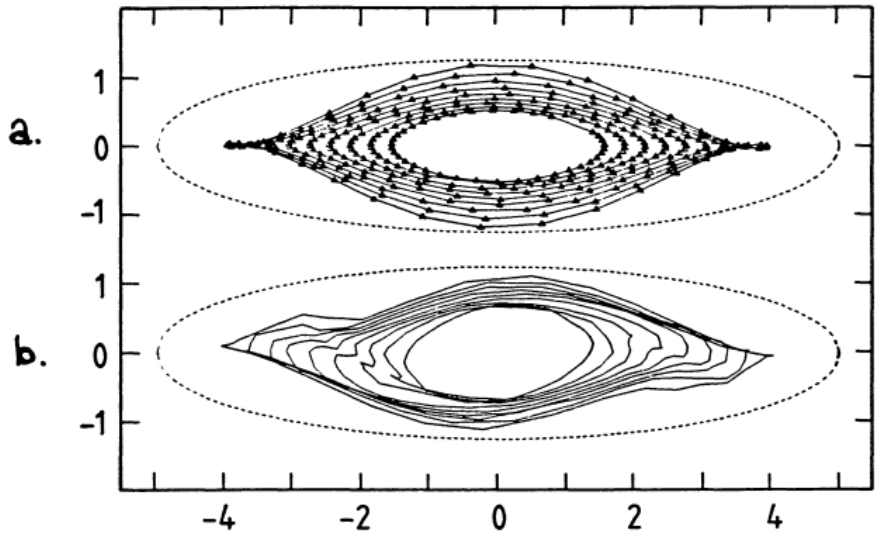

Figure 30: Representation of simulated of x_1 orbits in a strong bar, where high energy orbits develop loops at the ends of the bar as seen in Figure a. When bulk viscosity is added, the result is the arrange of orbits seen in Figure b. The looping orbits have collided with themselves and we can see that the higher energy orbits collide with lower energy orbits, causing shocks and forming the dust lanes we often encounter falling towards the centre. From Sanders et al. (1983)

Our second and third nuclear ring classes, 2 arms+ and many-armed rings, despite including some barred galaxies, are dominated by weakly barred and non barred galaxies respectively. Many-armed rings raise questions about their formation process, since the absence of a bar means that their formation can not be explained by the procedure described in Zurita et al. (2004). These rings are the most common in Flocculent galaxies, the intertwined and fragmented structure of these galaxies is much more uniform along the disc. This absence of a 180^{o} symmetry inhibits the appearance of any main dust lanes towards the centre. The study from Comerón et al. (2010) indicates that the nuclear ring formation mechanism in unbarred galaxies is strongly related to that in barred galaxies, quite possibly involving non-axisymmetry-induced resonances. These resonances could either be of a different nature than those caused by bars (such as assymmetries induced by interactions and spiral arms) or rather a remnant of the influence of a long gone, destroyed bar. The possible processes of bar weakening and/or destruction are explored in simulations like the ones described in Friedli & Benz (1993), Bournaud et al. (2005), Raha et al. (1991), Martinez-Valpuesta & Shlosman (2004) or Berentzen et al. (2007).

2 arms+ rings feature a weaker 180^{o} symmetry than two-armed rings but a stronger one than many-armed rings, as seen in Table 3. The presence and strength of a bar in the host galaxy that forces the existence of this symmetry has proven a key factor to determine the nature of the nuclear ring. Our study suggests that the different ring classes form a continuum with two-armed rings in one end and many-armed rings in the other, placing 2 arms+ rings as an intermediate case, defined

as:

- **two-armed rings**: 180^{o} structure forced by a strong bar.
- **2arms+ rings**: Weaker bars forcing a weaker 180^{o} structure.
- **many-armed rings**: Very weak or no 180^{o} structure, leads to the formation of many armlets.

5.3.2 Nuclear spirals

The unsharp-masking technique, when combined with high angular resolution, has shown itself to be extremely helpful to detect nuclear spirals. Using this method, we have detected 28 galaxies displaying nuclear dust spirals.

The sub-sample of galaxies with nuclear spirals shows no preference towards any particular stellar mass range or Hubble stage, although they more common in barred galaxies. In addition, they do show a tendency towards Grand Design galaxies and the least compact galaxies, but they can be found in every kind of galaxy. In fact, we find that they are present in almost every galaxy for which we had an *HST* image displaying the nuclear interior properly resolved available.

Nuclear spirals are described in Alig et al. (2023) as ubiquitous around black holes at the very low sub-Eddington regime, suggesting a direct correlation between these two phenomenons. Our study presents 28 galaxy candidates to present this kind of BH.

It is usual in the literature to separate the study of the nuclear region, and the study of the outer or larger scale structures of the galaxies. For instance, in Tully (1974), the author presents a detailed model to study and explain the spiral structure of M51 using a density wave hypothesis. The streaming motions that the author finds in this work are limited to the outside of the bar of the galaxy, and is hence unable to explain the structure within the innermost regions.

The aforementioned work by Prieto et al. (2005), that studies the nuclear region of NGC 1097, is continued in Prieto et al. (2019). There, the authors extend their analysis further out, at several kpc distance, and are then able to connect the nuclear spiral present within the ring with the dust, lane and filaments, outside of the ring and within the Inner Lindbald Resonance running parallel to the bar.

In this work, we present a way to extend the analysis further by following the dust filaments from the outermost to the innermost regions of the galaxy, thanks to the unsharp-masking technique. As shown in Fig. 31, we are able to follow the path of filaments -dark narrow regions in the figure- from the outer limits of the galaxy disk to the very central regions. These long and collimated structures defining a sort of inward spiral arms suggests that these may be pathways transporting material from the outer region of the galaxy straight to the centre, where the BH is located (Prieto et al. 2005). An in-depth study of the kinematics of the CO lines inside these regions would be essential to further develop the connections proposed here.

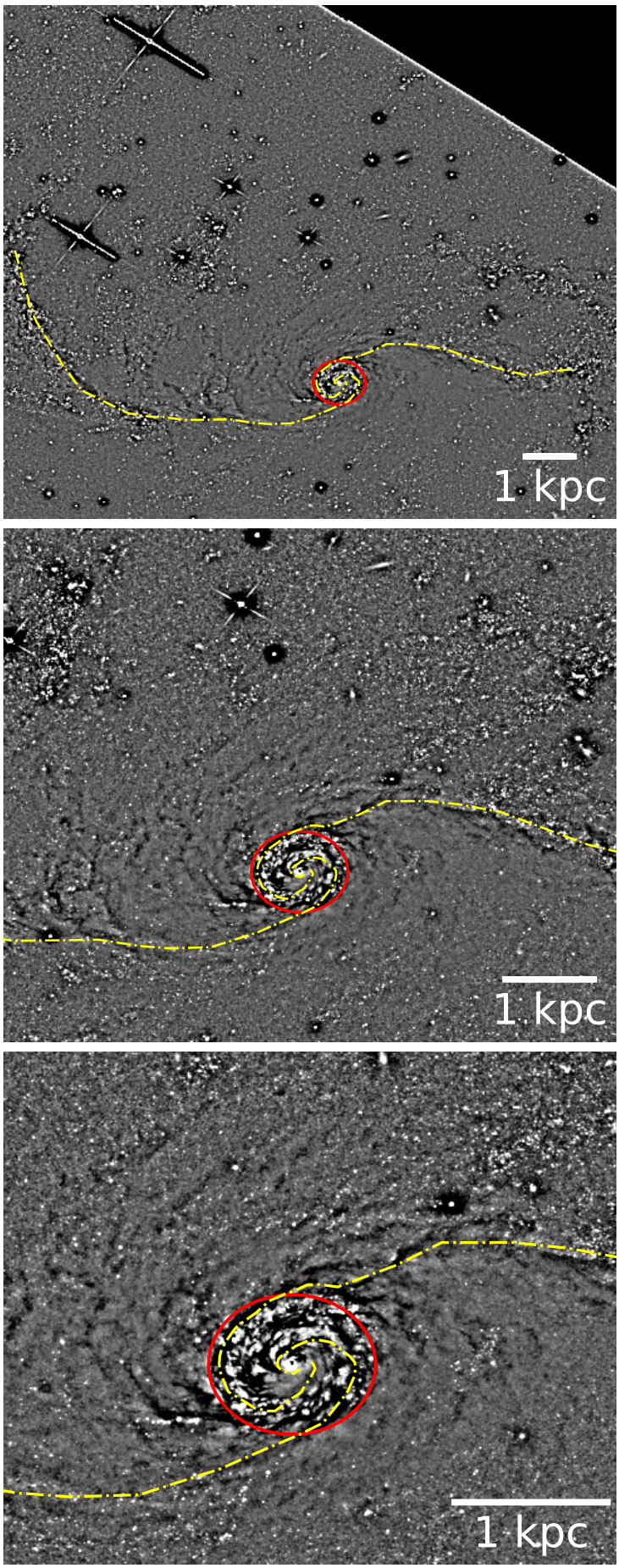

Figure 31: Unsharp-masked image of NGC 1672, displayed at different zoom levels, increasing from top to bottom. The dashed yellow lines follow the path of the dust towards the centre of the galaxy. The red circumference delineates the nuclear ring. The unsharp-masking allows us to trace the pathways of dust from the outer limits of the galaxy disk to the very central regions. North is up and East is left.

6 Conclusions

We have produced unsharp-masked images from *Hubble Space Telescope* archival data in the optical of a selection of 52 galaxies with nuclear rings from the Atlas of Images of NUclear Rings (AINUR) to study and characterise their structure.

We have grouped the galaxies into different classes within three different visual classifications. A first categorisation related to the morphology of the galaxy as a whole, dividing the sample in 11 Flocculent galaxies, 17 Multi-armed and 24 Grand Design galaxies. A second morphological classification attending to the arm structure, mainly arm density, around the nuclear ring and how open said structure is, sorting galaxies into most compact (14 galaxies), least compact (20 galaxies) and intermediate cases (18 galaxies). And finally, a classification based on the morphology of the nuclear ring itself that resulted in a distribution of 13 galaxies with two-armed rings that only show two dust lanes, 22 galaxies with 2 arms+ rings that feature two main dust lanes and additional smaller armlets and 17 galaxies presenting many-armed rings with multiple armlets leading into the ring. We used these classifications to infer correlations between galactic properties and nuclear ring structure.

We found that two-armed rings are more common in early type Grand design barred galaxies, whereas 2 arms+ rings are related to later type weakly barred galaxies, both Grand Design and Multiarmed, and many-armed rings are associated to later type non-barred Flocculent and Multiarmed galaxies.

We discovered that galaxies hosting two-armed rings present the strongest bars, the ones that host 2 arms+ rings have slightly weaker bars and many-armed rings appear in galaxies with very weak nonaxisymmetries. We conclude that the morphology of the host galaxy, and more precisely the presence and properties of a bar play a fundamental role in determining the morphology of the nuclear ring and the nuclear region.

In relation to this, our study suggests that the different ring classes form a continuum, governed by the influence of a 180^{o} symmetry present in the surroundings of the nuclear ring, with two-armed rings in one end and many-armed rings in the other, placing 2 arms+ rings as an intermediate case:

- **two-armed rings**: 180^{o} structure forced by a strong bar.
- **2arms+ rings**: Weaker bars forcing a weaker 180^{o} structure.
- **many-armed rings**: Very weak or no 180^{o} structure, leads to the formation of many armlets.

In addition, we made another classification on the basis of the presence of distinguishable nuclear features, mainly nuclear spirals, within the inside of the ring. We found nuclear spirals in 28 of the 32 galaxies from our sample for which we had an *HST* image displaying the interior of the nuclear ring properly resolved available. We can conclude that nuclear spirals seem a rather

common phenomenon in galaxies featuring nuclear rings, although a larger sample would provide a higher level of confidence in this claim.

We observed that the presence of nuclear spirals is not influenced by the presence or type of bar, Hubble class or stellar mass of the host galaxy. They are more frequent in the least compact and Grand Design galaxies and very rare in Flocculent galaxies. They also appear within nuclear rings of every kind, with a slight preference towards 2 arms+ rings. These long and collimated structures defining a sort of inward spiral arms suggests that these may be pathways transporting material from the outer region of the galaxy straight to the centre, where the BH is located.

The use of the unsharp-masking technique has proven very useful to study galactic structure from the outermost to the innermost regions. A more complete view of the nuclear regions and the processes that lead to the formation of nuclear structures would need a high angular resolution study of the kinematics, using for example the adaptive optics assisted mode of MUSE. In this work we have shown, statistically, that the overall morphology of the host galaxy can influence the morphology of the nuclear ring.

References

Alig, C., Prieto, A., Blaña, M., et al. 2023, The Astrophysical Journal, 953, 109

Athanassoula, E. 1992, MNRAS, 259, 345

Athanassoula, E. 1994, in Mass-Transfer Induced Activity in Galaxies, ed. I. Shlosman, 143

Barth, A. J., Ho, L. C., Filippenko, A. V., & Sargent, W. L. 1995, AJ, 110, 1009

Berentzen, I., Shlosman, I., Martinez-Valpuesta, I., & Heller, C. H. 2007, ApJ, 666, 189

Bournaud, F., Combes, F., & Semelin, B. 2005, MNRAS, 364, L18

Buta, R. 1986, The Astrophysical Journals, 61, 609

Buta, R. & Crocker, D. A. 1993, AJ, 105, 1344

Buta, R. J., Corwin, H. G., & Odewahn, S. C. 2007, The de Vaucouleurs Atlas of Galaxies

Buta, R. J., Sheth, K., Athanassoula, E., et al. 2015, The Astrophysical Journals, 217, 32

Combes, F. 1996, in Astronomical Society of the Pacific Conference Series, Vol. 91, IAU Colloq. 157: Barred Galaxies, ed. R. Buta, D. A. Crocker, & B. G. Elmegreen, 286

Combes, F. 2001, in Advanced Lectures on the Starburst-AGN, ed. I. Aretxaga, D. Kunth, & R. Mújica, 223

Combes, F. & Gerin, M. 1985, A&A, 150, 327

Combes, F. & Sanders, R. H. 1981, A&A, 96, 164

Comerón, S., Knapen, J. H., & Beckman, J. E. 2008, A&A, 485, 695

Comerón, S., Knapen, J. H., Beckman, J. E., et al. 2010, MNRAS, 402, 2462

Comerón, S., Knapen, J. H., Ramos Almeida, C., & Watkins, A. E. 2021, A&A, 645, A130

Curtis, H. D. 1918, Publications of Lick Observatory, 13, 9

de Vaucouleurs, G. 1959, Classification and Morphology of External Galaxies, ed. S. Flügge (Berlin, Heidelberg: Springer Berlin Heidelberg), 275–310

Elmegreen, B. G. & Elmegreen, D. M. 1985, The Astrophysical Journal, 288, 438

Elmegreen, B. G. & Elmegreen, D. M. 1989, The Astrophysical Journal, 342, 677

Elmegreen, D. M., Elmegreen, B. G., & Eberwein, K. S. 2002, The Astrophysical Journal, 564, 234

Elmegreen, D. M., Elmegreen, B. G., Yau, A., et al. 2011, The Astrophysical Journal, 737, 32

Englmaier, P. & Gerhard, O. 1997, MNRAS, 287, 57

Erwin, P. 2024, MNRAS, 528, 3613

Friedli, D. & Benz, W. 1993, A&A, 268, 65

Garcia-Barreto, J. A., Downes, D., Combes, F., et al. 1991, A&A, 244, 257

Heisler, C. A. & Vader, J. P. 1994, AJ, 107, 35

Ho, L. C., Filippenko, A. V., & Sargent, W. L. 1995, The Astrophysical Journals, 98, 477

Hubble, E. P. 1926, The Astrophysical Journal, 64, 321

Hubble, E. P. 1936, Realm of the Nebulae

Keeler, J. E. 1908, Publications of Lick Observatory, 8, 1

Kim, W.-T. & Elmegreen, B. G. 2017, ApJ, 841, L4

Kim, W.-T., Seo, W.-Y., Stone, J. M., Yoon, D., & Teuben, P. J. 2012, The Astrophysical Journal, 747, 60

Kim, Y. & Kim, W.-T. 2014, MNRAS, 440, 208

Knapen, J. H. 2005, A&A, 429, 141

Knapen, J. H., Allard, E. L., Mazzuca, L. M., Sarzi, M., & Peletier, R. F. 2006, Star formation in the central regions of galaxies

Knapen, J. H., Beckman, J. E., Heller, C. H., Shlosman, I., & de Jong, R. S. 1995, The Astrophysical Journal, 454, 623

Knapen, J. H., Pérez-Ramírez, D., & Laine, S. 2002, MNRAS, 337, 808

Malin, D. F. 1977, AAS Photo Bulletin, 16, 10

Maoz, D., Barth, A. J., Ho, L. C., Sternberg, A., & Filippenko, A. V. 2001, AJ, 121, 3048

Martinez-Valpuesta, I. & Shlosman, I. 2004, ApJ, 613, L29

May, D., Rodríguez-Ardila, A., Prieto, M. A., et al. 2018, MNRAS, 481, L105

Mazzuca, L. M., Knapen, J. H., Veilleux, S., & Regan, M. W. 2008, The Astrophysical Journals, 174, 337

Negroponte, J. & White, S. D. M. 1983, MNRAS, 205, 1009

Pogge, R. W. 1989, The Astrophysical Journals, 71, 433

Pogge, R. W. & Martini, P. 2002, The Astrophysical Journal, 569, 624

Prieto, M. A., Fernandez-Ontiveros, J. A., Bruzual, G., et al. 2019, MNRAS, 485, 3264

Prieto, M. A., Maciejewski, W., & Reunanen, J. 2005, The Astronomical Journal, 130, 1472

Prieto, M. A., Mezcua, M., Fernández-Ontiveros, J. A., & Schartmann, M. 2014, Monthly Notices of the Royal Astronomical Society, 442, 2145

Prieto, M. A., Nadolny, J., Fernández-Ontiveros, J. A., & Mezcua, M. 2021, Monthly Notices of the Royal Astronomical Society, 506, 562

Querejeta, M., Meidt, S. E., Schinnerer, E., et al. 2016, A&A, 588, A33

Raha, N., Sellwood, J. A., James, R. A., & Kahn, F. D. 1991, Nature, 352, 411

Reynaud, D. & Downes, D. 1998, A&A, 337, 671

Sandage, A. 1961, The Hubble Atlas of Galaxies

Sanders, R. H., Teuben, P. J., & van Albada, G. D. 1983, in Internal Kinematics and Dynamics of Galaxies, ed. E. Athanassoula, Vol. 100, 221

Schweizer, F. & Ford, W. K., J. 1985, in New Aspects of Galaxy Photometry, ed. J. L. Nieto, Vol. 232, 145

Sérsic, J. L. & Pastoriza, M. 1965, PASP, 77, 287

Sheth, K., Regan, M., Hinz, J. L., et al. 2010, PASP, 122, 1397

Sheth, K., Regan, M. W., Vogel, S. N., & Teuben, P. J. 2000, The Astrophysical Journal, 532, 221

Shlosman, I. 1999, in Astronomical Society of the Pacific Conference Series, Vol. 187, The Evolution of Galaxies on Cosmological Timescales, ed. J. E. Beckman & T. J. Mahoney, 100–114

Shlosman, I., Begelman, M. C., & Frank, J. 1990, Nature, 345, 679

Shlosman, I., Frank, J., & Begelman, M. C. 1989, Nature, 338, 45

Storchi-Bergmann, T., Dors, Oli L., J., Riffel, R. A., et al. 2007, The Astrophysical Journal, 670, 959

Tully, R. B. 1974, The Astrophysical Journals, 27, 449

van de Ven, G. & Chang, P. 2009, The Astrophysical Journal, 697, 619

Zurita, Relaño, M., Beckman, J. E., & Knapen, J. H. 2004, AA, 413, 73

Appendix A Unsharp-masked images

Unsharp-masked images from the *HST* images of the galaxies in our sample. The galaxy ID appears in the top-left corner. The sigma in pixels of the Gaussian kernel used to produce the unsharp-masked image appears in the bottom-right corner. The bar in the top-right corner shows the angular size of 1 kpc. The red ellipse indicates the nuclear ring in the galaxy. North is up and east is left.

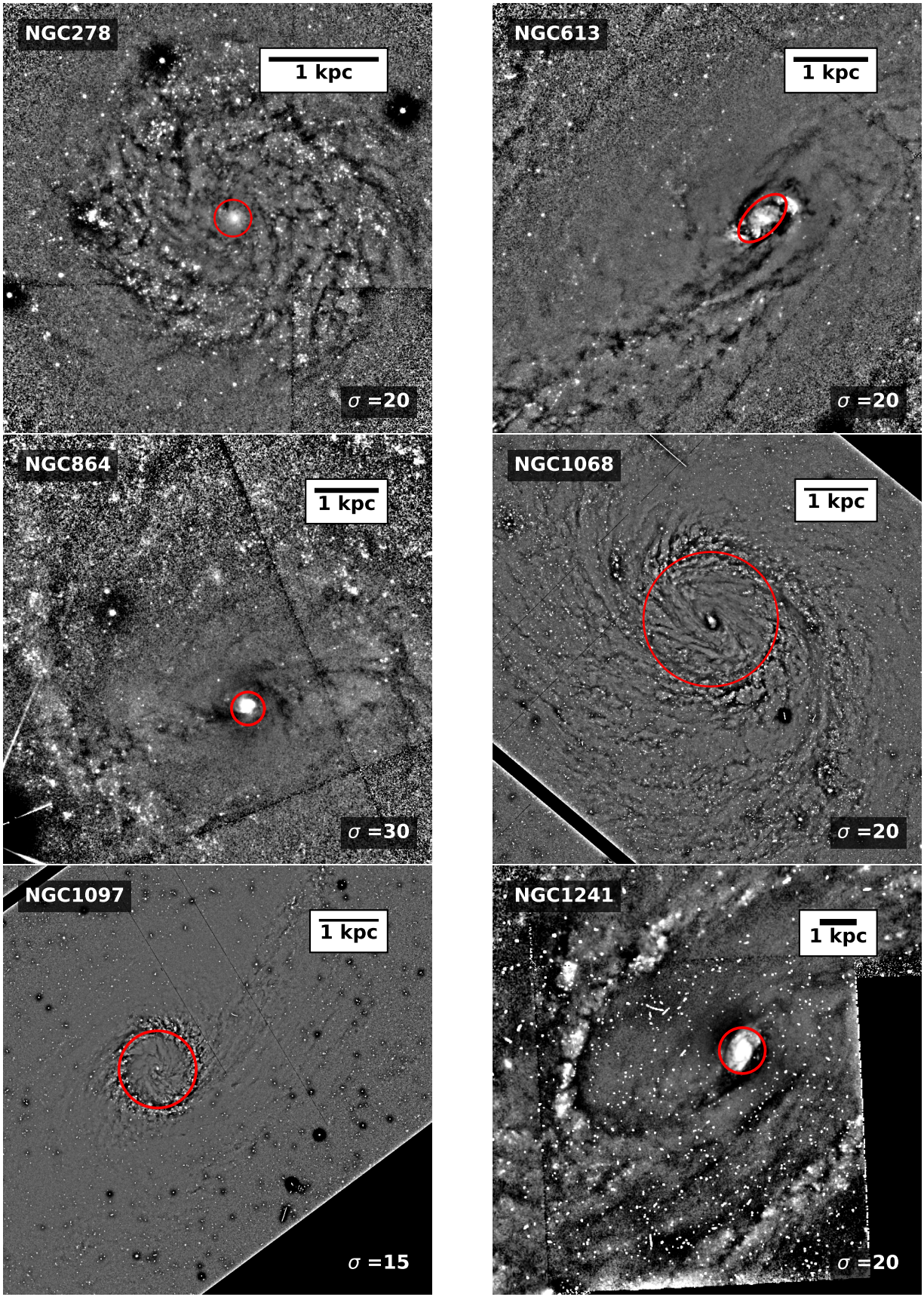
NGC278
1 kpc
σ =20
NGC613
1 kpc
σ =20
NGC864
1 kpc
σ =30
NGC1068
1 kpc
σ =20
NGC1097
1 kpc
σ =15
NGC1241
1 kpc
σ =20

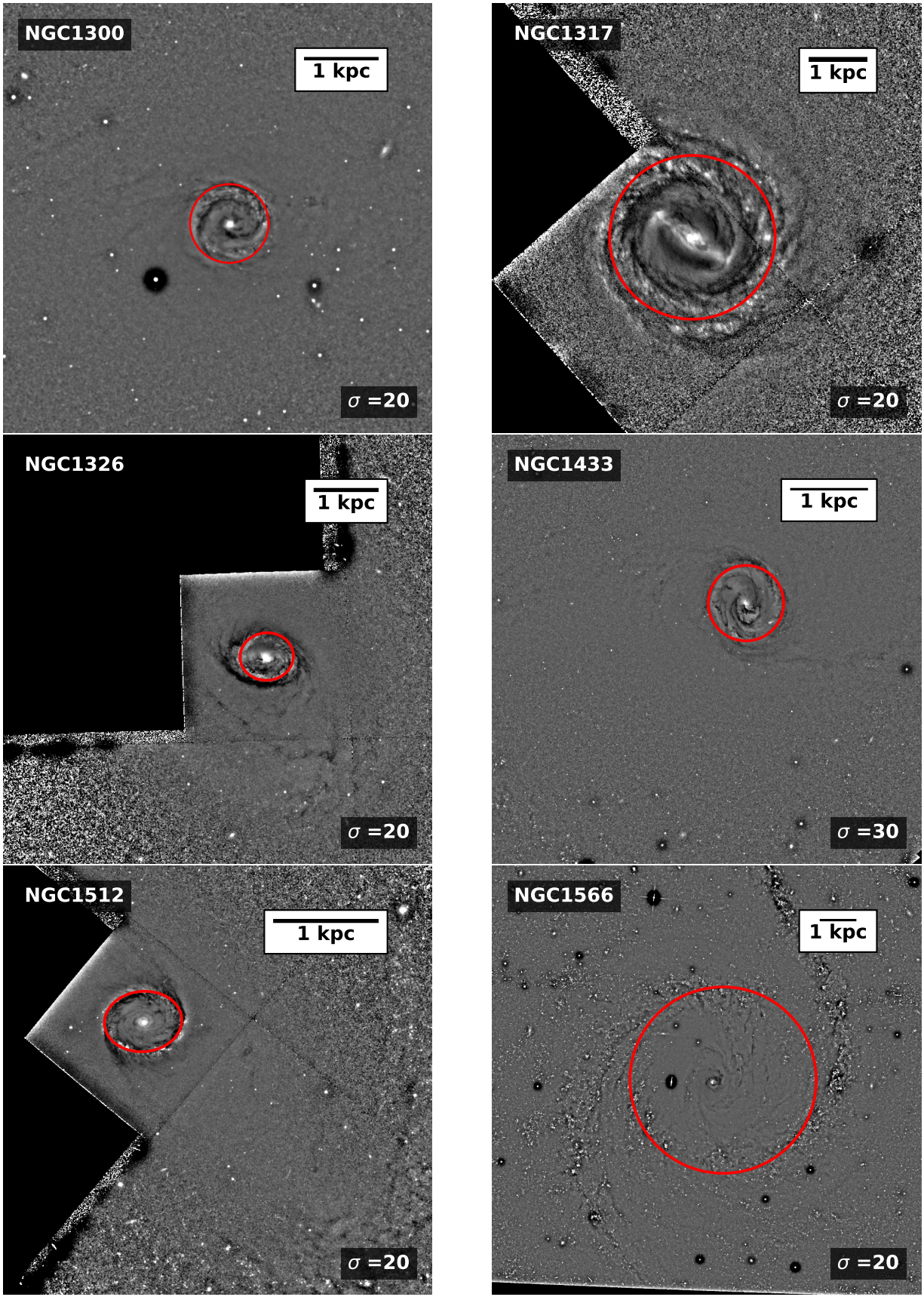
NGC1300
1 kpc
σ =20
NGC1317
1 kpc
σ =20
NGC1326
1 kpc
σ =20
NGC1433
1 kpc
σ =30
NGC1512
1 kpc
σ =20
NGC1566
1 kpc
σ =20

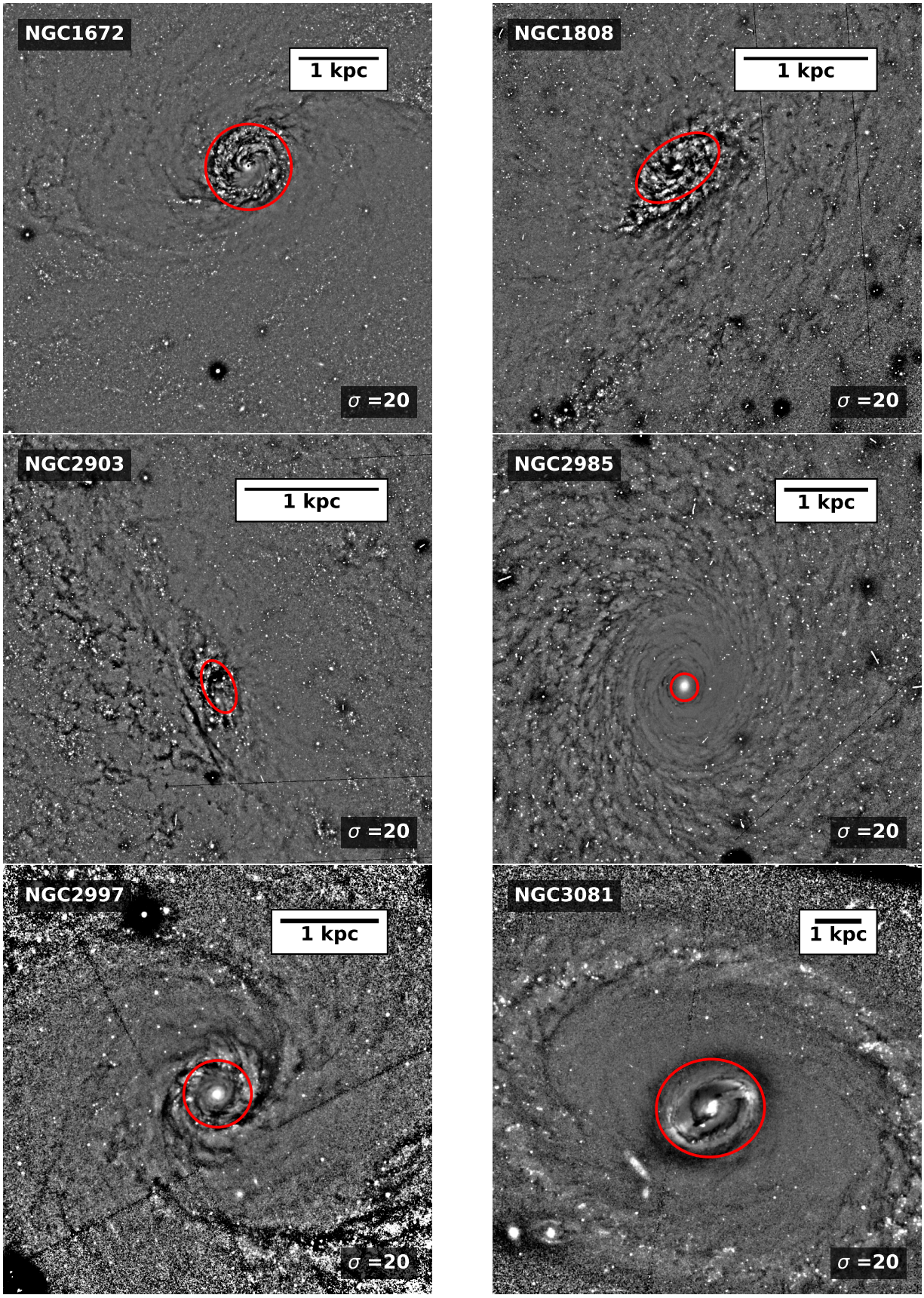
NGC1672
1 kpc
σ =20
NGC1808
1 kpc
σ =20
NGC2903
1 kpc
σ =20
NGC2985
1 kpc
σ =20
NGC2997
1 kpc
σ =20
NGC3081
1 kpc
σ =20

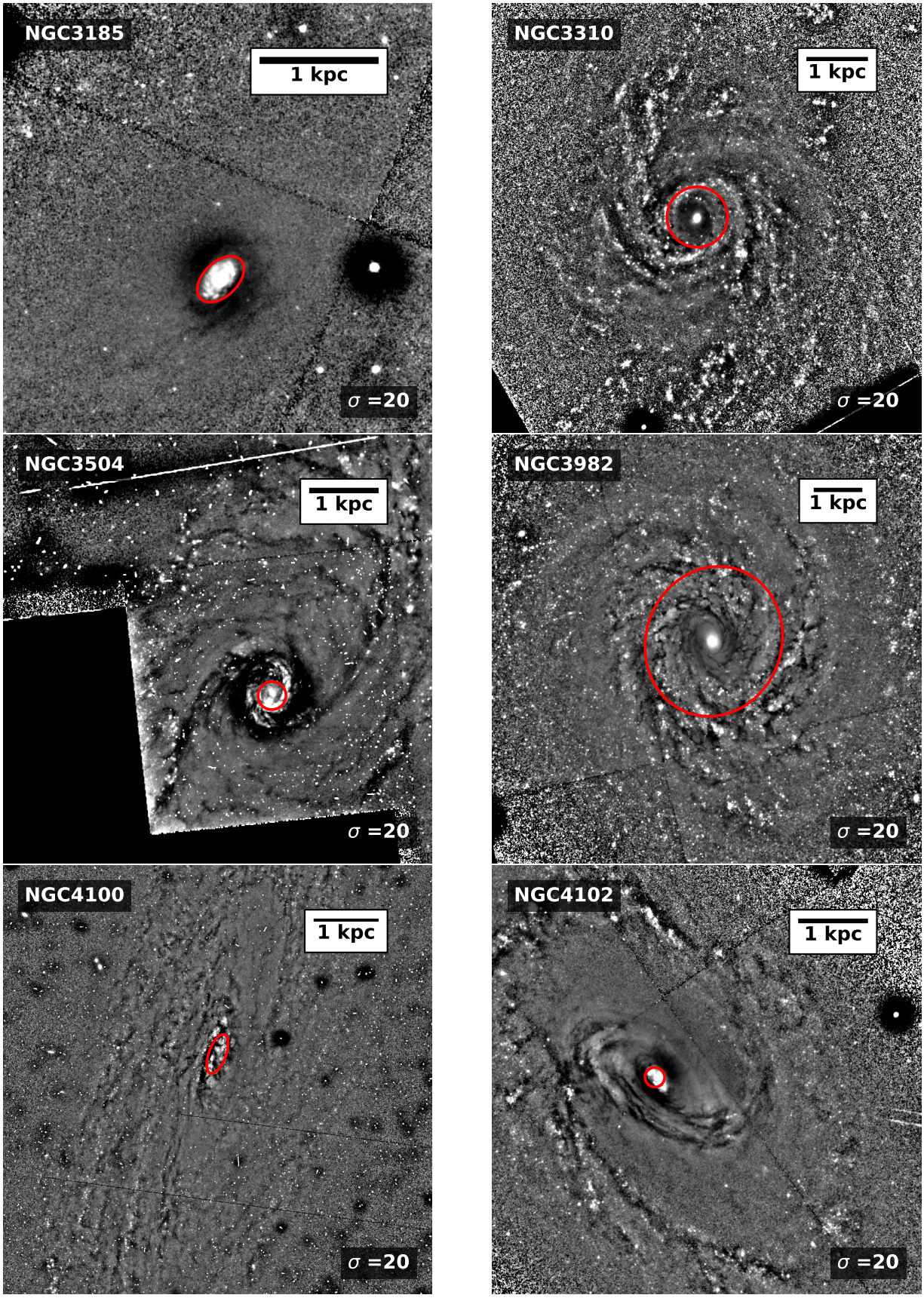
NGC3185
1 kpc
σ =20
NGC3310
1 kpc
σ =20
NGC3504
1 kpc
σ =20
NGC3982
1 kpc
σ =20
NGC4100
1 kpc
σ =20
NGC4102
1 kpc
σ =20

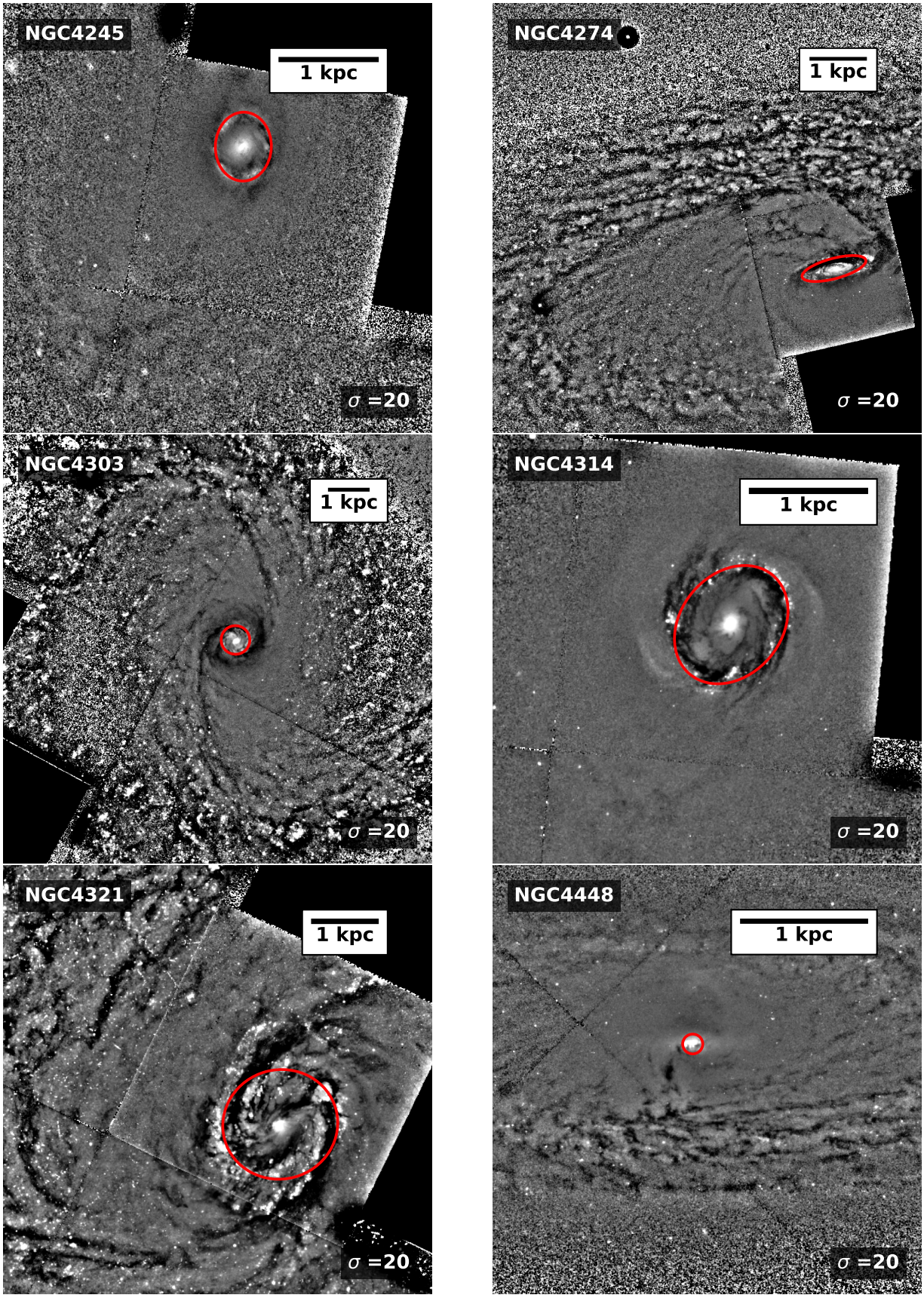
NGC4245
1 kpc
σ =20
NGC4274
1 kpc
σ =20
NGC4303
1 kpc
σ =20
NGC4314
1 kpc
σ =20
NGC4321
1 kpc
σ =20
NGC4448
1 kpc
σ =20

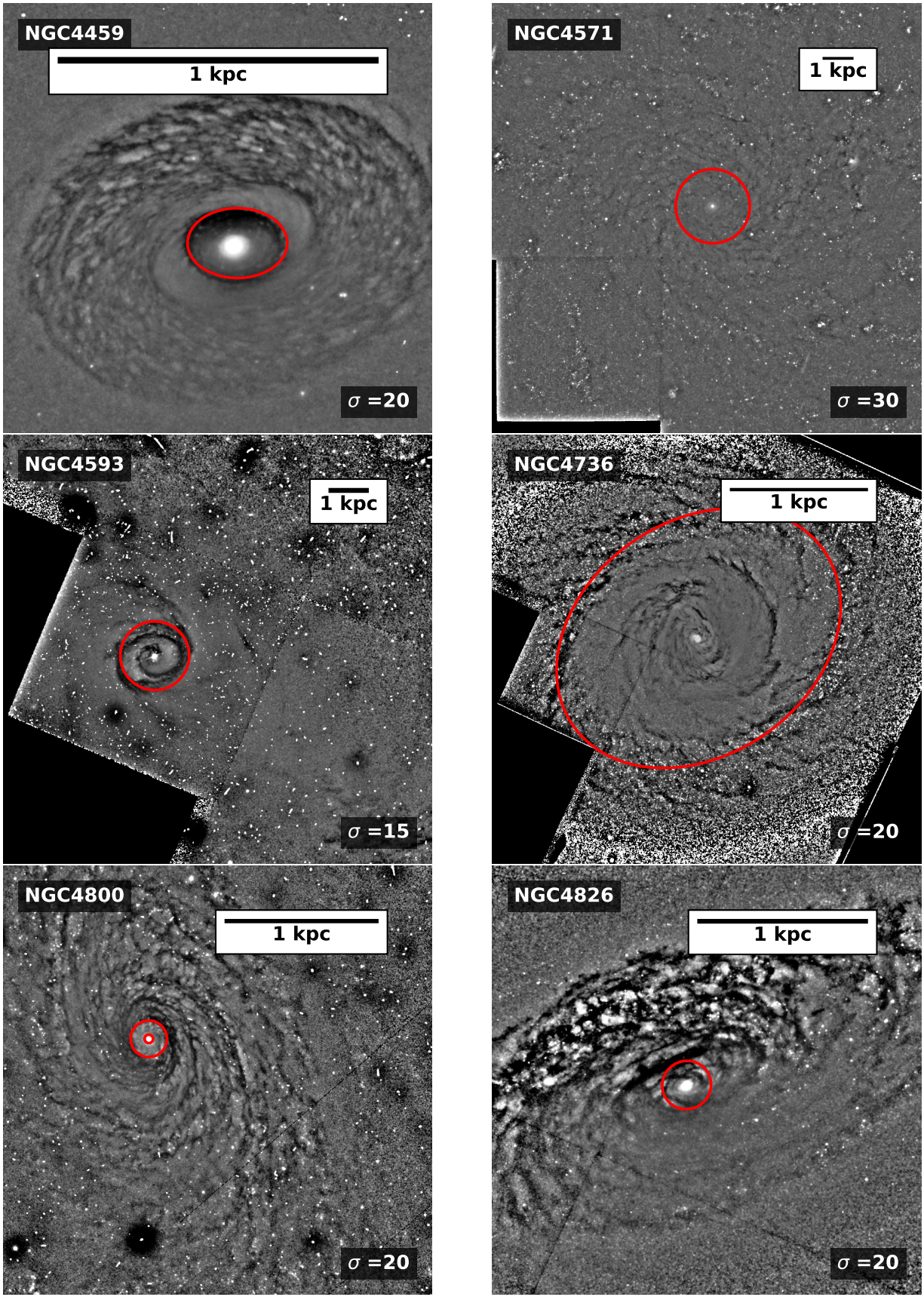
NGC4459
1 kpc
σ =20
NGC4571
1 kpc
σ =30
NGC4593
1 kpc
σ =15
NGC4736
1 kpc
σ =20
NGC4800
1 kpc
σ =20
NGC4826
1 kpc
σ =20

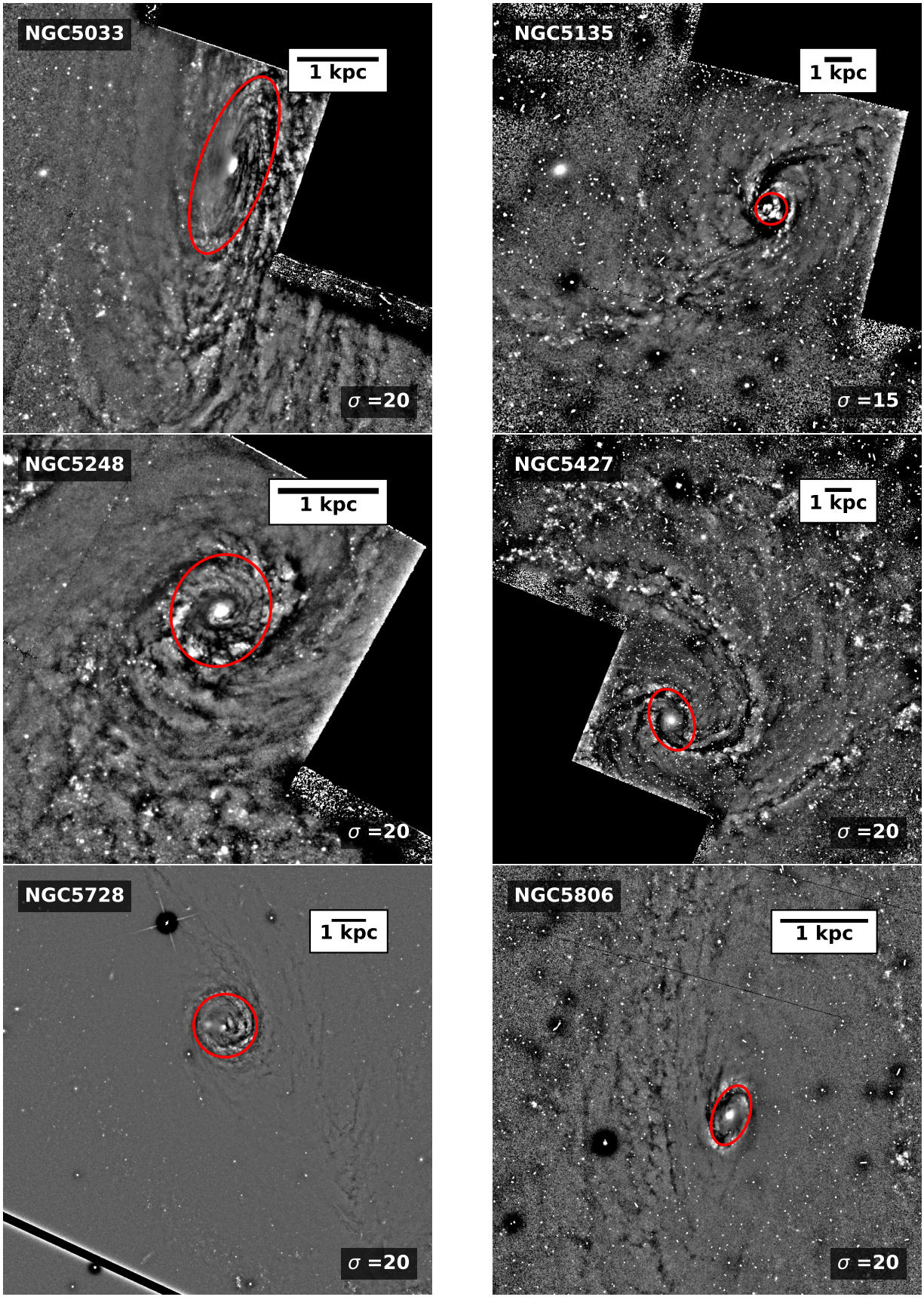
NGC5033
1 kpc
σ =20
NGC5135
1 kpc
σ =15
NGC5248
1 kpc
σ =20
NGC5427
1 kpc
σ =20
NGC5728
1 kpc
σ =20
NGC5806
1 kpc
σ =20

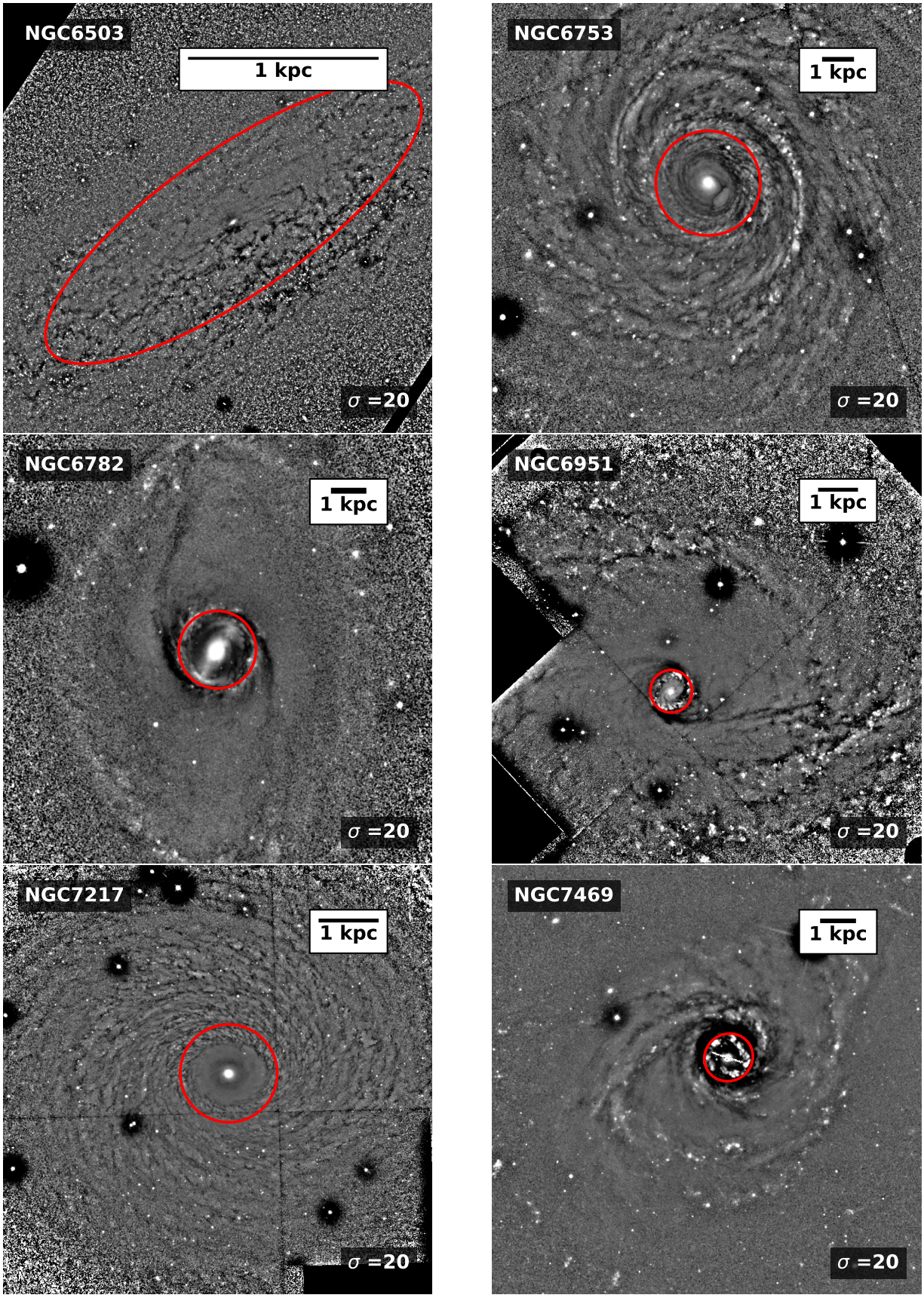
NGC6503
1 kpc
σ =20
NGC6753
1 kpc
σ =20
NGC6782
1 kpc
σ =20
NGC6951
1 kpc
σ =20
NGC7217
1 kpc
σ =20
NGC7469
1 kpc
σ =20

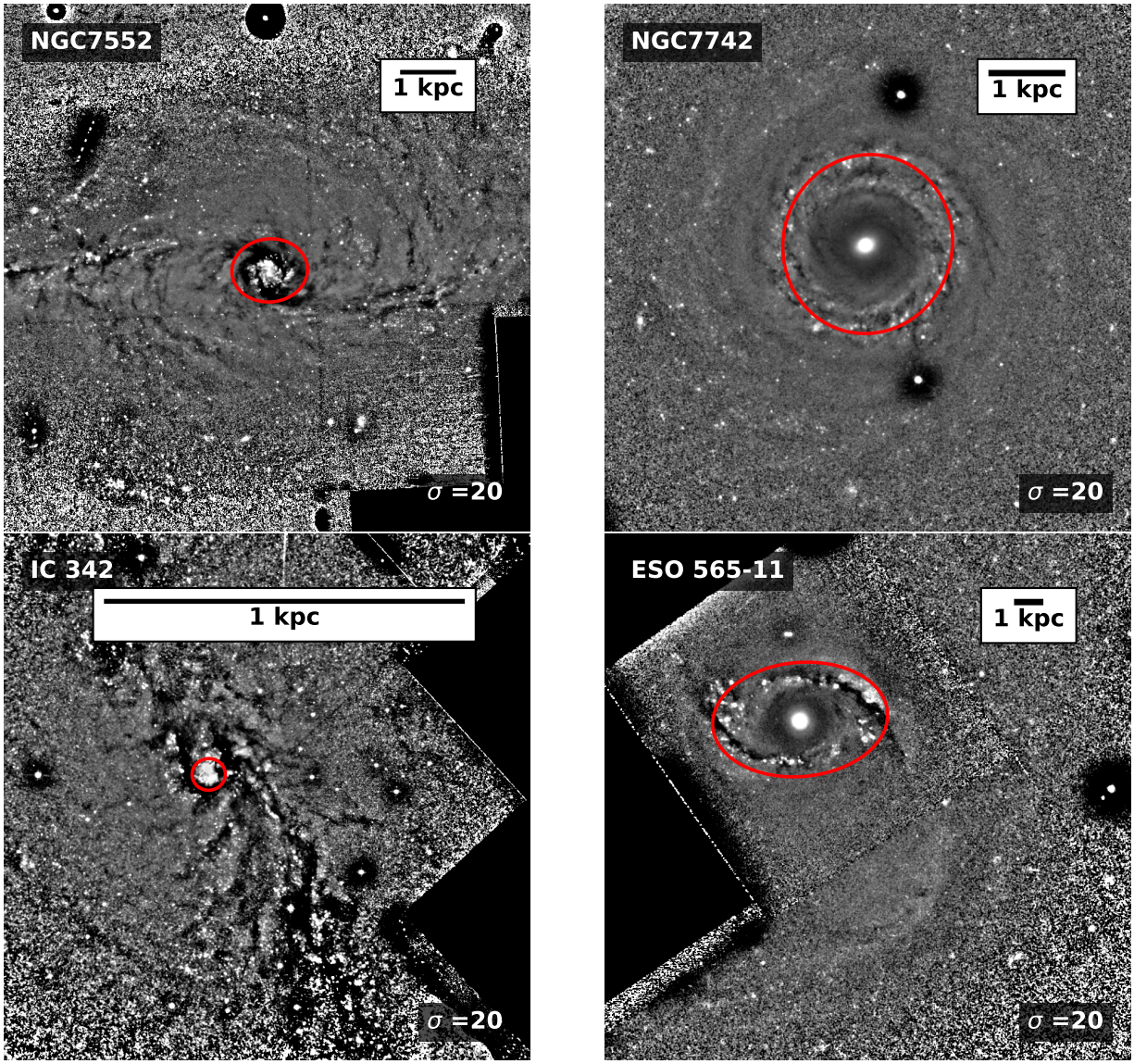
NGC7552
1 kpc
σ =20
NGC7742
1 kpc
σ =20
IC 342
1 kpc
σ =20
ESO 565-11
1 kpc
σ =20